# Critical dynamics in mixtures

R. Folk[1] and G. Moser[2]
[1]*Institute for Theoretical Physics, University of Linz, Austria*
[2]*Institute for Physics and Biophysics, University of Salzburg, Salzburg, Austria*
(Received 15 June 1998)

We derive the nonasymptotic expressions for the frequency- and temperature-dependent sound velocity and sound absorption near a critical point in a mixture within renormalization group theory in one-loop order. The dynamic model considered is an extension of the corresponding model for pure fluids including concentration fluctuations. The theoretical result for the complex sound velocity is the same as at consolute points and gas-liquid critical points reflecting universality. Differences observed in the experiments at the two critical points mentioned are due to the different behavior of the sound velocity at $T_c$, which is finite in mixtures and zero in pure fluids, as well as due to nonasymptotic effects. Near the consolute point we compare our result with the phenomenological theory of Ferrell and Bhattacharjee [Phys. Rev. B **24**, 4095 (1981); Phys. Rev. A **31**, 1788 (1985)] and near the gas-liquid critical point with experiments in the $^3$He-$^4$He mixture. A genuine dynamic parameter not considered so far and related to the critical enhancement of the thermal conductivity appears in the nonasymptotic expressions of the transport coefficients and the complex sound velocity. All nonuniversal background parameters of the complex sound velocity are fixed by a comparison of the corresponding theoretical expressions for the transport coefficients with experiments. [S1063-651X(98)10711-0]

PACS number(s): 64.70.Fx, 64.60.Ht

## I. INTRODUCTION

This paper continues our calculation of nonasymptotic transport properties within renormalization group (RG) theory near critical points in fluids and mixtures. In Ref. [1] the dynamics of pure fluids was considered including sound propagation. Here we extend the theory to mixtures near a consolute point, as well as near a plait point (gas-liquid critical point). All these critical points belong to the same universality class of model *H* [2], although the nonuniversal behavior may be different [3]. Moreover, one does not always reach asymptotics within the experimental region and in order to compare with experiments a nonasymptotic theory describing the crossover to the background behavior is needed [4].

Regarding the transport coefficients such as mass diffusion, thermal conductivity, thermal diffusion ratio, and shear viscosity, mainly mode coupling theory or variants have been used to describe the nonasymptotic behavior near the critical points. At a plait point the mode coupling theory has recently been further developed in Ref. [5]; the decoupled mode theory was used in Refs. [6–9]. RG results were already used for the comparison in $^3$He-$^4$He mixtures near the plait point in Refs. [10,11]. Near the consolute point several mixtures have been considered in Ref. [12] and the enhancement of the thermal conductivity in butoxyethanol-water mixtures could be accounted for [13].

The critical sound propagation near a consolute point has been described by Ferrell and Bhattacharjee within a phenomenological theory based on a generalization of the specific heat to finite frequencies taking into account the causal and scaling properties of the dynamic functions involved [14,15]. An earlier application of the RG theory to critical sound at the consolute point used a reduced model neglecting, e.g., the thermal diffusion ratio [16]. Recently, Onuki used the bulk viscosity [17] for an intuitive derivation of the critical sound behavior [18] that is in agreement with our RG calculations [19].

Critical effects in transport properties near a second-order phase transition are usually described by stochastic equations neglecting the sound mode. It is well established that universal quantities such as the critical exponents, in particular the dynamic critical exponent *z*, are not affected by the sound mode. This is not generally true for nonasymptotic properties. As an example we mention the superfluid transition in $^4$He, where additional terms are present in the thermal conductivity when the sound mode is coupled to the other hydrodynamic modes and the order parameter [20]. Near the critical point in a pure liquid no additional contributions appear [1].

The paper is organized as follows. In Sec. II we define the static Hamiltonian and the stochastic model equations. Then the relation between the model vertex functions and the hydrodynamic transport coefficients is derived in Secs. III A and III B. The expressions for the sound mode are presented in Sec. III C. Then in Sec. IV we compare our theoretical results with experiment. In Sec. IV A we analyze the shear viscosity near consolute and plait points for aniline-cyclohexane mixtures and $^3$He-$^4$He mixtures, respectively. Taking the dynamic parameters found in comparison with experimental data, we predict the sound velocity and attenuation near a plait point in Sec. IV B. Other hydrodynamic transport coefficients are compared with experiment in Sec. IV C. A comparison of our result with the phenomenological theory of Ferrell and Bhattacharjee is contained in Sec. V. A discussion is given in Sec. VI. In Appendixes A–E further details of the theoretical calculations are given.

## II. MODEL

The critical behavior of the hydrodynamic transport coefficients corresponding to the slow heat and mass diffusion

 

modes at the plait point and at the consolute point have been investigated recently [10,3,11]. These investigations have been performed in a reduced model $H'$ based on the considerations of [2], where the fast mode describing the critical sound propagation has been neglected, although in [3] a complete model including the sound propagation has already been derived. This model, which is applicable at the plait point as well as at the consolute point, is the basis for the considerations in the present work.

### A. Statics

The derivation of the static functional, which determines the critical behavior of the thermodynamic derivatives, proceeds in the following three steps, performed explicitly in [3] and summarized here.

(i) According to methods in nonequilibrium statistical thermodynamics [21], a local probability density has been introduced, which is defined by an internal energy density, the kinetic energy density, and the local conserved densities (all densities per volume). In liquid mixtures the local conserved densities include the entropy density $s(x)$, the mass densities $\rho_3(x),\rho_4(x)$ of the two constituents of the mixture (e.g., $^3$He and $^4$He), and the momentum current $\mathbf{j}'(x)$. The conjugated local intensive fields are the temperature $T(x)$, the chemical potentials of the two constituents $\mu_3(x),\mu_4(x)$, and the velocity $\mathbf{v}(x)$. Instead of $\rho_3(x),\rho_4(x)$ one also can use $\rho_3(x)$ and the mass density $\rho(x)=\rho_3(x)+\rho_4(x)$ as local densities when the corresponding intensive fields $\mu_3(x)$ and $\mu_4(x)$ are changed to $\mu_4(x)$ and the chemical potential difference $\Delta(x)=\mu_3(x)-\mu_4(x)$. Assuming that the local densities are fluctuating around their thermodynamic average values, they may be written as $\alpha(x)=\alpha+\Delta\alpha(x)$ with $\alpha=s,\rho_3,\rho,\mathbf{j}'$, where $\Delta$ denotes the fluctuating part. The local thermodynamic potential is then divided into an equilibrium part and a part containing the contributions from the fluctuations. A static functional is obtained by expanding the fluctuation contribution into powers of the conserved densities. The correlations of the conserved densities are related to thermodynamic derivatives (specific heat, compressibility, etc.) at fixed intensive fields $T$, $\Delta$, $\mu_4$, and $\mathbf{v}$.

(ii) Instead of the field $\mu_4$ it is more convenient to introduce the experimental accessible field, the pressure $P$. This can be achieved by introducing the entropy per mass $\sigma(x)=s(x)/\rho(x)$ and the mass concentration $c(x)=\rho_3(x)/\rho(x)$ in the static functional. The fluctuations of the densities per volume will then be replaced by $\Delta s(x)=\rho\Delta\sigma(x)+\sigma\Delta\rho(x)$ and $\Delta\rho_3(x)=\rho\Delta c(x)+c\Delta\rho(x)$. These new densities have the advantage that they also appear in the hydrodynamic theory.

(iii) In the next step we have to distinguish between the plait point and the consolute point since only the order parameter $\phi_0$ has to be taken into account in fourth order. The order parameter is then decoupled from the remaining two densities (the momentum density trivially decouples from all other densities), which then represent secondary densities $\vec{q}_0^{\,T}=(\mathring{q}_1,\mathring{q}_2)$ in the quadratic part. This decoupling is obtained by a shift of the order parameter and a restriction of the secondary densities to a subspace with fixed order parameter. A third-order term quadratic in the order parameter and linear in the two other densities remains.

At the plait point the entropy per mass fluctuation is chosen as the order parameter

$$\phi_0(x)=\sqrt{N_A}[\Delta\sigma(x)-\langle\Delta\sigma(x)\rangle], \tag{2.1}$$

while at the consolute point the concentration fluctuation represents the order parameter

$$\phi_0(x)=\sqrt{N_A}[\Delta c(x)-\langle\Delta c(x)\rangle]. \tag{2.2}$$

The secondary densities are defined as

$$\vec{q}_0(x)=\sqrt{N_A}\Delta\vec{y}(x)-\vec{Q}\phi_0(x), \tag{2.3}$$

where $\vec{y}^{\,T}=(c,\rho)$ and $\vec{Q}=(\partial\vec{y}/\partial\sigma)_{\Delta,P}$ at the plait point, and $\vec{y}^{\,T}=(\sigma,\rho)$ and $\vec{Q}=(\partial\vec{y}/\partial c)_{T,P}$ at the consolute point. The Avogadro number $N_A$ has been introduced for convenience to turn the Boltzmann constant $k_B$ into the gas constant $R$ in all expressions.

Now both cases can be treated by one form of the static functional

$$\begin{aligned}H=\int d^dx\Big\{&\frac{1}{2}\,\mathring{\tau}\phi_0^2(x)+\frac{1}{2}\,[\boldsymbol{\nabla}\phi_0(x)]^2\\&+\frac{1}{2}\,\vec{q}_0^{\,T}(x)\overleftrightarrow{A}\vec{q}_0(x)+\frac{1}{2}\,a_j\mathbf{j}^2(x)+\frac{\mathring{\overset{\circ}{u}}}{4!}\,\phi_0^4(x)\\&+\frac{1}{2}\,\mathring{\vec{\gamma}}_q^{\,T}\vec{q}_0(x)\phi_0^2(x)-\mathring{\vec{h}}_q^{\,T}\vec{q}_0(x)\Big\}.\end{aligned} \tag{2.4}$$

The overcircle on the parameters and the subscript 0 on the densities denote unrenormalized quantities. The static functional has the same structure as in pure liquids [1], but now with two secondary densities $\vec{q}_0^{\,T}=(\mathring{q}_1,\mathring{q}_2)$. As a consequence, the parameters

$$\overleftrightarrow{A}=\begin{pmatrix}a_{11}&a_{12}\\a_{12}&a_{22}\end{pmatrix},\quad \mathring{\vec{\gamma}}_q=\begin{pmatrix}\mathring{\gamma}_1\\\mathring{\gamma}_2\end{pmatrix},\quad \mathring{\vec{h}}_q=\begin{pmatrix}\mathring{h}_1\\\mathring{h}_2\end{pmatrix} \tag{2.5}$$

are matrices and vectors instead of scalars. The momentum density appearing in Eq. (2.4) is also rescaled by the Avogadro number $\mathbf{j}=\sqrt{N_A}\Delta\mathbf{j}'$. The parameter $a_j$ follows from the expression for the kinetic energy and reads $a_j=1/RT\rho$. The coefficients of the matrix $\overleftrightarrow{A}$ are the lowest-order contributions to the static two-point vertex functions and therefore do not contain critical effects. They are related to background values of thermodynamic derivatives at the plait and the consolute point, respectively. Their explicit values are given in Appendix A.

A static functional of the same structure as Eq. (2.4) is used in the renormalization group theory of the λ transition in $^3$He-$^4$He mixtures [22,23] without coupling to the sound mode and at the λ transition in pure $^4$He when the first sound propagation is included [20]. The treatment of Eq. (2.4) is therefore well known and the main relations used in the following are briefly summarized.

Since the static critical behavior of mixtures belongs to the same universality class as pure fluids the critical properties derived with Eq. (2.4) can be related to those of the $\phi^4$ model [24]. These relations are found by eliminating the sec-

ondary densities, which is possible since they appear only up to second order. The coefficients of the remaining $\phi^4$ model

$$H_\phi = \int d^dx \left\{ \frac{1}{2}\,\mathring{r}\,\phi_0^2(x) + \frac{1}{2}\,[\nabla\phi_0(x)]^2 + \frac{\mathring{u}}{4!}\,\phi_0^4(x) \right\} \tag{2.6}$$

are related to the parameters in Eq. (2.4) by

$$\mathring{u} = \mathring{\tilde{u}} - 3\,\mathring{\vec{\gamma}}_q^T \overleftrightarrow{A}^{-1} \mathring{\vec{\gamma}}_q\,, \quad \mathring{r} = \mathring{\tau} + \mathring{\vec{\gamma}}_q^T \overleftrightarrow{A}^{-1} \mathring{\vec{h}}_q\,. \tag{2.7}$$

A consequence of the reducibility of Eq. (2.4) is that the correlations of the secondary densities $\vec{q}_0$ are related to order parameter correlation functions. For the expectation value and the two-point correlation function one gets

$$\langle \vec{q}_0 \rangle = \overleftrightarrow{A}^{-1} (\mathring{\vec{h}}_q - \mathring{\vec{\gamma}}_q \langle \tfrac{1}{2}\phi_0^2 \rangle), \tag{2.8}$$

$$\langle \vec{q}_0 \otimes \vec{q}_0 \rangle_c = \overleftrightarrow{A}^{-1} + \mathring{\vec{\delta}}_q \otimes \mathring{\vec{\delta}}_q \langle \tfrac{1}{2}\phi_0^2 \tfrac{1}{2}\phi_0^2 \rangle_c\,. \tag{2.9}$$

$\mathring{\vec{\delta}}_q = \overleftrightarrow{A}^{-1} \mathring{\vec{\gamma}}_q$ has been introduced in Eq. (2.9). The subscript $c$ in Eq. (2.9) denotes the cummulant $\langle \alpha\beta \rangle_c = \langle \alpha\beta \rangle - \langle \alpha \rangle \langle \beta \rangle$. Note that the correlations on the left-hand sides of Eqs. (2.8) and (2.9) are calculated with the static functional containing Eq. (2.4), while on the right-hand side Eq. (2.6) is used. Therefore, the $\phi^2$ correlations are functions of $\mathring{u}$ only. All secondary density correlation functions in Eq. (2.9) contain the same singular order parameter correlation function. This correlation function may be eliminated in two of the equations by inserting the third one. As a result, one gets two relations between the background parameters

$$a_{11} - \frac{\mathring{\gamma}_1}{\mathring{\gamma}_2}\,a_{12} = k_1\,, \quad a_{22} - \frac{\mathring{\gamma}_2}{\mathring{\gamma}_1}\,a_{12} = k_2\,. \tag{2.10}$$

$k_1$, $k_2$, and the ratio of the two $\gamma$ couplings may be expressed by thermodynamic derivatives along the critical line comparing the corresponding thermodynamic relations. These derivatives are smooth functions of the temperature, finite at $T_c$, and therefore will be treated as constants in the critical region. Their connection to thermodynamic derivatives is given in Appendix A. From the static functional (2.4) it follows that the secondary densities $\vec{q}_0$ have finite expectation values. In order to perform the perturbation expansion it is convenient to introduce conjugated external fields $\mathring{\vec{h}}_q$ in Eq. (2.4). The values of $\mathring{\vec{h}}_q$ are then adjusted to eliminate the expectation values of $\vec{q}_0$. Equation (2.8) implies that the conjugated external fields have to be $\mathring{\vec{h}}_q = \mathring{\vec{\gamma}}_q \langle \tfrac{1}{2}\phi_0^2 \rangle$.

The Fourier transformed correlation functions of the densities at the wave vector $k=0$,

$$\langle \alpha\beta \rangle_c \equiv \langle \alpha\beta \rangle_c (k=0) = \int d^dx \langle \alpha(x)\beta(0) \rangle_c = \int d^dx \langle \Delta\alpha(x)\Delta\beta(0) \rangle_c\,, \tag{2.11}$$

with $\alpha, \beta = \phi_0, \mathring{q}_1, \mathring{q}_2$, are related to thermodynamic derivatives containing the critical singularities. The order parameter correlation is related to a strongly divergent (exponent $\gamma$) thermodynamic derivative, while the secondary densities correspond to weakly divergent (exponent $\alpha$) thermodynamic derivatives. The relations for the plait point and the consolute point are presented in Appendix A. The momentum density separates into a longitudinal component $\mathbf{j}_l(x)$, with the property $\nabla \times \mathbf{j}_l(x) = 0$, and an orthogonal transverse component $\mathbf{j}_t(x)$, with $\nabla \mathbf{j}_l(x) = 0$. Thus the quadratic momentum density fluctuations in Eq. (2.4) may be written as $\mathbf{j}^2(x) = \mathbf{j}_l^2(x) + \mathbf{j}_t^2(x)$.

### B. Dynamics

From generalized Poisson bracket relations [25] and the dissipative properties of liquid mixtures in hydrodynamics [26] a set of dynamic equations has been derived [3], which allows the calculation of critical sound propagation effects. It represents an extension of model $H'$ [2], where only the slow heat and concentration diffusion modes are included. The equations read

$$\frac{\partial \phi_0}{\partial t} = \mathring{\Gamma} \nabla^2 \frac{\delta H}{\delta \phi_0} + \mathring{\vec{L}}_q^T \nabla^2 \frac{\delta H}{2\vec{q}_0} - \mathring{g}(\nabla\phi_0) \left( \frac{\delta H}{\delta \mathbf{j}_l} + \frac{\delta H}{\delta \mathbf{j}_t} \right) + \Theta_\phi\,, \tag{2.12}$$

$$\frac{\partial \vec{q}_0}{\partial t} = \mathring{\vec{L}}_q \nabla^2 \frac{\delta H}{\delta \phi_0} + \mathring{\vec{\Lambda}}_q \nabla^2 \frac{\delta H}{\delta \vec{q}_0} - \mathring{g}(\nabla \vec{q}_0) \left( \frac{\delta H}{\delta \mathbf{j}_l} + \frac{\delta H}{\delta \mathbf{j}_t} \right) - (\mathring{\vec{c}}_q + \mathring{\vec{g}}_l \phi_0 + \mathring{\overleftrightarrow{g}}_q \vec{q}_0) \nabla \frac{\delta H}{\delta \mathbf{j}_l} + \vec{\Theta}_q\,, \tag{2.13}$$

$$\frac{\partial \mathbf{j}_l}{\partial t} = \mathring{\lambda}_l \nabla^2 \frac{\delta H}{\delta \mathbf{j}_l} - \mathring{\vec{c}}_q^T \nabla \frac{\delta H}{\delta \vec{q}_0} - \mathring{\vec{g}}_l^T \nabla \left( \phi_0 \frac{\delta H}{\delta \vec{q}_0} \right) - \nabla \left( \vec{q}_0^T \mathring{\overleftrightarrow{g}}_q \frac{\delta H}{\delta \vec{q}_0} \right) + \mathring{g}(1-\mathcal{T}) \left[ (\nabla\phi_0) \frac{\delta H}{\delta \phi_0} + (\nabla \vec{q}_0)^T \frac{\delta H}{\delta \vec{q}_0} \right] - \mathring{g}(1-\mathcal{T}) \sum_k \left[ j_k \nabla \frac{\delta H}{\delta j_k} - \nabla_k \mathbf{j} \frac{\delta H}{\delta j_k} \right] + \mathbf{\Theta}_l\,, \tag{2.14}$$

$$\frac{\partial \mathbf{j}_t}{\partial t} = \mathring{\lambda}_t \nabla^2 \frac{\delta H}{\delta \mathbf{j}_t} + \mathring{g}\mathcal{T} \left[ (\nabla\phi_0) \frac{\delta H}{\delta \phi_0} + (\nabla \vec{q}_0)^T \frac{\delta H}{\delta \vec{q}_0} \right] - \mathring{g}\mathcal{T} \sum_k \left[ j_k \nabla \frac{\delta H}{\delta j_k} - \nabla_k \mathbf{j} \frac{\delta H}{\delta j_k} \right] + \Theta_t\,, \tag{2.15}$$

where $\mathcal{T}$ is the projector to the direction of the transverse momentum density. The static functional $H$ is given by Eq. (2.4). Assuming a Markovian process, the fluctuating forces $[\Theta_i]^T = (\Theta_\phi, \vec{\Theta}_q^T, \Theta_l, \Theta_t)$ fullfill the Einstein relations

$$\langle [\Theta_i](x,t) \otimes [\Theta_j](x',t') \rangle = 2[\Lambda_{ij}] \delta(t-t')\,\delta(x-x')\,, \tag{2.16}$$

with the matrix

$$[\Lambda_{ij}]$$

$$= \begin{pmatrix} -\mathring{\Gamma}\nabla^2 & -\mathring{\vec{L}}_q^T\nabla^2 & 0 & 0 \\ -\mathring{\vec{L}}_q\nabla^2 & -\mathring{\vec{\Lambda}}_q\nabla^2 & 0 & 0 \\ 0 & 0 & -\mathring{\lambda}_l\nabla^2 & 0 \\ 0 & 0 & 0 & -\mathring{\lambda}_t\nabla^2 \end{pmatrix}. \quad (2.17)$$

The Onsager coefficient vector and the Onsager coefficient matrix in Eqs. (2.12) and (2.13) are

$$\mathring{\vec{L}}_q = \begin{pmatrix} \mathring{L} \\ \mathring{L}_\phi \end{pmatrix}, \quad \mathring{\vec{\Lambda}}_q = \begin{pmatrix} \mathring{\mu} & \mathring{L}_{12} \\ \mathring{L}_{12} & \mathring{\lambda} \end{pmatrix}. \quad (2.18)$$

The mode coupling vectors and the mode coupling matrix introduced in Eqs. (2.13) and (2.14) are defined as

$$\mathring{\vec{c}}_q = \begin{pmatrix} 0 \\ \mathring{c} \end{pmatrix}, \quad \mathring{\vec{g}}_l = \begin{pmatrix} 0 \\ \mathring{g}_l \end{pmatrix}, \quad \mathring{\vec{g}}_g = \begin{pmatrix} 0 & 0 \\ 0 & \mathring{g} \end{pmatrix}, \quad (2.19)$$

with the parameters $\mathring{c} = RT\rho$, $\mathring{g} = RT/\sqrt{N_A}$, and $\mathring{g}_l = RTQ_2/\sqrt{N_A}$. The Onsager coefficients in the momentum density equations (2.14) and (2.15) are related to the background values of the shear viscosity $\overline{\eta}^{(0)}$ and the bulk viscosity $\zeta^{(0)}$ by $\mathring{\lambda}_l = RT(\zeta^{(0)} + \frac{4}{3}\overline{\eta}^{(0)})$ and $\mathring{\lambda}_t = RT\overline{\eta}^{(0)}$.

In hydrodynamics only three transport coefficients, the thermal conductivity $\kappa_T$, the thermal diffusion coefficient $k_T$, and the mass diffusion coefficient $D$, appear in the equations for the entropy and the concentration. The hydrodynamic equation for the mass density is the continuity equation, which does not involve any dissipation. As a consequence, only three ($\mathring{\Gamma}$, $\mathring{L}$, and $\mathring{\mu}$) of the six Onsager coefficients in Eqs. (2.12)–(2.15) are independent. The remaining three coefficients result from the transformation (2.3) and they are determined by

$$\mathring{L}_\phi = -Q_2\mathring{\Gamma}, \quad \mathring{\lambda} = Q_2^2\mathring{\Gamma}, \quad \mathring{L}_{12} = -Q_2\mathring{L}. \quad (2.20)$$

Consequently, the fluctuating forces in Eq. (2.16) are not independent. Nevertheless, a dynamic functional analogous to [27] may be derived [1].

The hydrodynamic Onsager coefficients $\alpha$, $\beta$, and $\gamma$ determine the mass current **i** and heat current **q** as a function of the temperature gradient and the chemical potential gradient [26]:

$$\mathbf{i} = -\beta\boldsymbol{\nabla}T - \alpha\boldsymbol{\nabla}\Delta, \quad \mathbf{q} - \Delta\mathbf{i} = -\gamma\boldsymbol{\nabla}T - T\beta\boldsymbol{\nabla}\Delta. \quad (2.21)$$

These coefficients are related to the hydrodynamic transport coefficients by

$$\alpha = \rho\left(\frac{\partial c}{\partial\Delta}\right)_{T,P}^{(0)} D^{(0)}, \quad (2.22)$$

$$\beta = \rho D^{(0)}\left[\frac{k_T^{(0)}}{T} + \left(\frac{\partial c}{\partial T}\right)_{\Delta,P}^{(0)}\right], \quad (2.23)$$

$$\gamma = \kappa_T^{(0)} + \rho T D^{(0)}\left(\frac{\partial\Delta}{\partial c}\right)_{T,P}^{(0)}\left[\frac{k_T^{(0)}}{T} + \left(\frac{\partial c}{\partial T}\right)_{\Delta,P}^{(0)}\right]^2. \quad (2.24)$$

At the plait point the independent model Onsager coefficients $\mathring{\Gamma}$, $\mathring{L}$, and $\mathring{\mu}$ are related to the hydrodynamic coefficients by

$$\mathring{\Gamma} = \frac{R\gamma}{\rho^2}, \quad \mathring{L} = \frac{RT}{\rho^2}\left(\beta - \frac{\gamma}{T}Q_1\right), \quad (2.25)$$

$$\mathring{\mu} = \frac{RT}{\rho^2}\left(\alpha - 2\beta Q_1 + \frac{\gamma}{T}Q_1^2\right). \quad (2.26)$$

At the consolute point one has

$$\mathring{\Gamma} = \frac{RT\alpha}{\rho^2}, \quad \mathring{L} = \frac{RT}{\rho^2}(\beta - \alpha Q_1), \quad (2.27)$$

$$\mathring{\mu} = \frac{RT}{\rho^2}\left(\frac{\gamma}{T} - 2\beta Q_1 + \alpha Q_1^2\right). \quad (2.28)$$

In the present model Eqs. (2.22)–(2.24) are used in the noncritical background indicated by (0) at the thermodynamic derivatives and hydrodynamic transport coefficients. In mode coupling theories [28,5] the same relations are extended into the critical region by replacing the background values by the corresponding fully divergent quantities.

### C. Elimination of one static coupling $\gamma$

Equations (2.8) and (2.9) are basic relations in the extended static model (2.4) because they show that all singularities in the extended static model are determined by the singularities of the $\phi^4$ model. Therefore, these relations have to be invariant under renormalization, which means that they have to be valid also for the renormalized quantities. However, this implies a matrix structure of the renormalization coefficients [23]. In order to avoid this matrix renormalization it is convenient to introduce transformed secondary densities $\mathring{\vec{m}}^T = (\mathring{m}_1, \mathring{m}_2)$ where only one density (for instance, $\mathring{m}_2$) is coupled to the order parameter, while the second density appears only in quadratic order in the static functional. This introduces densities ''orthogonal'' and ''parallel'' to the critical line. Whereas all quantities corresponding to the uncoupled density are considered along a path parallel to the critical line and therefore are finite (constant in the small critical region), the quantities corresponding to the remaining density are considered along a path perpendicular to the critical line containing critical singularities [29]. The new densities are introduced by a transformation

$$\mathring{\vec{m}} = \overleftrightarrow{M}\mathring{\vec{q}}, \quad \overleftrightarrow{M} = \begin{pmatrix} M_{11} & M_{12} \\ M_{21} & M_{22} \end{pmatrix}, \quad (2.29)$$

where the components of the matrix are determined by three conditions: (i) the nondiagonal coefficient of the Gaussian part in the transformed static functional has to vanish, (ii) the $\gamma$ coupling of $\mathring{m}_1$ has to vanish, and (iii) $\det(\overleftrightarrow{M}) = 1$. The resulting matrix coefficients are

$$M_{11}=1, \quad M_{22}=\frac{k_1}{k_1+\left(\frac{\mathring{\gamma}_1}{\mathring{\gamma}_2}\right)^2 k_2},$$

$$M_{21}=\frac{\mathring{\gamma}_1}{\mathring{\gamma}_2} M_{22}, \quad M_{12}=\frac{\mathring{\gamma}_1}{\mathring{\gamma}_2}\frac{k_2}{k_1}, \tag{2.30}$$

where $k_1$ and $k_2$ have been introduced in Eq. (2.10). The transformation matrix may be expressed by thermodynamic derivatives using Table VII. The explicit expressions depending on the type of the critical point are listed in Appendix A. The transformed static functional obtained by inserting Eq. (2.29) into Eq. (2.4) reads

$$H=\int d^dx\Big\{\frac{1}{2}\,\mathring{\tau}\phi_0^2(x)+\frac{1}{2}\,[\boldsymbol{\nabla}\phi_0(x)]^2 + \frac{1}{2}\,a_1 m_1^2(x)+\frac{1}{2}\,a_2\mathring{m}_2^2(x)+\frac{1}{2}\,a_j\mathbf{j}^2(x)+\frac{\tilde{u}}{4!}\,\phi_0^4(x) + \frac{1}{2}\,\mathring{\gamma}_m\mathring{m}_2(x)\phi_0^2(x)-\mathring{h}_m\mathring{m}_2(x)\Big\}. \tag{2.31}$$

The secondary densities are decoupled in Eq. (2.31); therefore, the corresponding correlation functions are simply determined by

$$\langle\mathring{m}_1\mathring{m}_1\rangle_c=\frac{1}{a_1}, \quad \langle\mathring{m}_1\mathring{m}_2\rangle_c=0\,, \tag{2.32}$$

$$\langle\mathring{m}_2\mathring{m}_2\rangle_c=\frac{1}{\mathring{\Gamma}_{m_2m_2}}=\frac{1}{a_2}\left(1+\frac{\mathring{\gamma}_m^2}{a_2}\left\langle\frac{1}{2}\,\phi_0^2\,\frac{1}{2}\,\phi_0^2\right\rangle_c\right), \tag{2.33}$$

where $\mathring{\Gamma}_{m_2m_2}$ is a static two-point vertex function containing only one-particle irreducible contributions. The second equality in Eq. (2.33) follows from Eq. (2.9). From the thermodynamic expressions for the coefficients of the matrix $\overleftrightarrow{A}$, the correlation functions, and the transformation matrix $\overleftrightarrow{M}$, the corresponding thermodynamic expressions of the transformed correlation functions (2.32) and (2.33) can be calculated, which are also given explicitely in Appendix A for the plait point and the consolute point. The transformation (2.29) leads to dynamic equations of the same structure as Eqs. (2.12)–(2.15), but with transformed Onsager coefficients and mode couplings

$$\vec{\mathring{L}}_m=\begin{pmatrix}\mathring{L}\\ \mathring{L}_\phi\end{pmatrix}=\overleftrightarrow{M}\vec{\mathring{L}}_q, \quad \overleftrightarrow{\mathring{\lambda}}_m=\begin{pmatrix}\mathring{\mu} & \mathring{L}_{12}\\ \mathring{L}_{12} & \mathring{\lambda}\end{pmatrix}=\overleftrightarrow{M}\overleftrightarrow{\mathring{\Lambda}}_q\overleftrightarrow{M}^T, \tag{2.34}$$

$$\vec{\mathring{g}}_l=\begin{pmatrix}\mathring{g}_{l1}\\ \mathring{g}_{l2}\end{pmatrix}=\overleftrightarrow{M}\vec{\mathring{g}}_l, \quad \overleftrightarrow{\mathring{g}}_m=\begin{pmatrix}\mathring{g}_{11} & \mathring{g}_{12}\\ \mathring{g}_{21} & \mathring{g}_{22}\end{pmatrix}=\overleftrightarrow{M}\overleftrightarrow{\mathring{g}}_q\overleftrightarrow{M}^{-1}, \tag{2.35}$$

$$\vec{\mathring{c}}_m=\begin{pmatrix}\mathring{c}_1\\ \mathring{c}_2\end{pmatrix}=\overleftrightarrow{M}\vec{\mathring{c}}_q\,. \tag{2.36}$$

## III. THEORETICAL RESULTS

### A. General relations

In order to identify the hydrodynamic transport coefficients one has to relate them to certain two-point vertex functions, calculated within a perturbation expansion of the dynamic functional given in Appendix B. We proceed as in the case of pure liquids [1] considering the hydrodynamic determinant $\Delta_H$. The linearized hydrodynamic equations in mixtures read (we use the notation of [26])

$$\frac{\partial\sigma}{\partial t}=\left\{\frac{Dk_T}{T}\left(\frac{\partial\Delta}{\partial c}\right)_{T,P}\left[\frac{k_T}{T}+\left(\frac{\partial c}{\partial T}\right)_{\Delta,P}\right]+\frac{x_T}{\rho T}\right\}\nabla^2 T + D\left(\frac{\partial\Delta}{\partial c}\right)_{T,P}\left[\frac{k_T}{T}+\left(\frac{\partial c}{\partial T}\right)_{\Delta,P}\right]\left[\nabla^2 c-\left(\frac{\partial c}{\partial P}\right)_{T,\Delta}\nabla^2 P\right], \tag{3.1}$$

$$\frac{\partial c}{\partial t}=\frac{Dk_T}{T}\,\nabla^2 T+D\nabla^2 c-D\left(\frac{\partial c}{\partial P}\right)_{T,\Delta}\nabla^2 P, \tag{3.2}$$

$$\frac{\partial\rho}{\partial t}=-\boldsymbol{\nabla}\mathbf{j}_l\,, \tag{3.3}$$

$$\frac{\partial\mathbf{j}_l}{\partial t}=-\boldsymbol{\nabla}P+\frac{1}{\rho}\left(\zeta+\frac{4}{3}\,\overline{\eta}\right)\nabla^2\mathbf{j}_l\,, \tag{3.4}$$

$$\frac{\partial\mathbf{j}_t}{\partial t}=\frac{\overline{\eta}}{\rho}\,\nabla^2\mathbf{j}_t\,. \tag{3.5}$$

Equations (3.1)–(3.5) include three diffusion modes and one sound mode. Fourier transforming the above equations and calculating the coefficient determinant to lowest order of $\omega$ and $k^2$, one gets

$$\Delta_H=(-i\omega+D_tk^2)[-\omega^2-(D+D_c)i\omega k^2 + DD_Tk^4](\omega^2-c_s^2k^2+D_si\omega k^2), \tag{3.6}$$

with the diffusion coefficients defined as

$$D_t=\frac{\overline{\eta}}{\rho}, \quad D_T=\frac{\kappa_T}{\rho C_{Pc}}, \quad D_c=D_T+\frac{Dk_T^2}{\rho C_{Pc}}\left(\frac{\partial\Delta}{\partial c}\right)_{T,P}, \tag{3.7}$$

where $C_{Pc}=T(\partial\sigma/\partial T)_{c,P}$ is the isobaric specific heat at constant concentration. $D_T$ and $D_c$ are two different types of thermal diffusion coefficients. $D_T$ denotes the thermal diffusion at mass flow zero ($\mathbf{i}=\mathbf{0}$), whereas $D_c$ denotes it at zero concentration gradient ($\boldsymbol{\nabla}c=\mathbf{0}$). The sound velocity $c_s$ and the sound diffusion coefficient $D_s$ in the sound mode are

$$c_s^2=\left(\frac{\partial P}{\partial\rho}\right)_{\sigma,c}, \tag{3.8}$$

$$D_s=\frac{1}{\rho}\left(\zeta+\frac{4}{3}\overline{\eta}\right)+\left(\frac{1}{C_{Vc}}-\frac{1}{C_{Pc}}\right)\frac{\kappa_T}{\rho}+\frac{D}{\rho^2}\left(\frac{\partial P}{\partial\rho}\right)_{\sigma,c}\left(\frac{\partial\Delta}{\partial c}\right)_{T,P}\left[\left(\frac{\partial\rho}{\partial\Delta}\right)_{T,P}+\left(\frac{\partial\rho}{\partial\sigma}\right)_{c,P}\frac{k_T}{T}\right]^2, \tag{3.9}$$

with the isochoric specific heat $C_{Vc}=T(\partial\sigma/\partial T)_{c,\rho}$. Equation (3.6) has to be compared with the determinant of the dynamical two-point vertex function of the model equations in the hydrodynamic limit ($\omega\to 0$, $k\to 0$) keeping the lowest orders in the frequency and the wave vector. We defer the definitions of these vertex functions to Appendix B. However, it should be mentioned that the structure of the expressions obtained is the same at the plait point and at the consolute point and that it is invariant under the transformation of the secondary densities from $\vec{q}_0$ to $\vec{m}_0$ [Eq. (2.29)]. Calculating the determinant of the matrix (B17), one gets the following structure, which is quite similar to Eq. (3.6):

$$\Delta_{th}=(-i\omega+\mathcal{D}_t k^2)[-\omega^2-(\mathcal{D}'+\mathcal{D}'')i\omega k^2+\mathcal{D}'\mathcal{D}''k^4](\omega^2-\mathcal{C}_s^2k^2+\mathcal{D}_s i\omega k^2). \tag{3.10}$$

The difference is that the coefficients in Eq. (3.10), obtained by collecting contributions of the corresponding powers in $k$ and $\omega$, are now complex quantities in general. One has

$$\mathcal{C}_s^2=-[\mathring{G}_{\tilde{\alpha}}]^T[\mathring{G}_\alpha], \tag{3.11}$$

$$\mathcal{D}_s=\mathring{f}_{ll\tilde{}}+\frac{[\mathring{G}_{\tilde{\alpha}}]^T[\mathring{\underline{F}}_{\alpha\tilde{\alpha}}][\mathring{G}_\alpha]}{[\mathring{G}_{\tilde{\alpha}}]^T[\mathring{G}_\alpha]}, \tag{3.12}$$

$$\mathcal{D}'+\mathcal{D}''=\mathrm{Tr}[\mathring{\underline{F}}_{\alpha\tilde{\alpha}}]-\frac{[\mathring{G}_{\tilde{\alpha}}]^T[\mathring{\underline{F}}_{\alpha\tilde{\alpha}}][\mathring{G}_\alpha]}{[\mathring{G}_{\tilde{\alpha}}]^T[\mathring{G}_\alpha]}, \tag{3.13}$$

$$\mathcal{D}'\mathcal{D}''=\mathring{\mathcal{F}}_{\alpha\tilde{\alpha}}\mathrm{Tr}[\mathring{\underline{F}}_{\alpha\tilde{\alpha}}]-\mathring{\Pi}_F+\frac{[\mathring{G}_{\tilde{\alpha}}]^T[\mathring{\underline{F}}_{\alpha\tilde{\alpha}}]^2[\mathring{G}_\alpha]}{[\mathring{G}_{\tilde{\alpha}}]^T[\mathring{G}_\alpha]}, \tag{3.14}$$

$$\mathcal{D}_t=\mathring{f}_{t\tilde{t}}. \tag{3.15}$$

In Eq. (3.14) the quantities $\mathring{\mathcal{F}}_{\alpha\tilde{\alpha}}$ and $\mathring{\Pi}_F$ are defined by

$$\mathring{\mathcal{F}}_{\alpha\tilde{\alpha}}=\mathrm{Tr}[\mathring{\underline{F}}_{\alpha\tilde{\alpha}}]-\mathring{f}_{\phi\tilde{\phi}}-\frac{[\mathring{G}_{\tilde{\alpha}}]^T[\mathring{\underline{F}}_{\alpha\tilde{\alpha}}][\mathring{G}_\alpha]}{[\mathring{G}_{\tilde{\alpha}}]^T[\mathring{G}_\alpha]}, \tag{3.16}$$

$$\mathring{\Pi}_F=\mathrm{Tr}\vec{\vec{\mathring{F}}}^2_{\alpha\tilde{\alpha}}+\det\vec{\vec{\mathring{F}}}_{\alpha\tilde{\alpha}}-\vec{\vec{\mathring{F}}}^T_{\tilde{\alpha}}\vec{\vec{\mathring{F}}}_{\alpha\alpha}. \tag{3.17}$$

The vectors $[\mathring{G}_\alpha]$,$[\mathring{G}_{\tilde{\alpha}}]$ and the matrix $[\mathring{\underline{F}}_{\alpha\tilde{\alpha}}]$ are introduced in Eqs. (B17)–(B20). Analogously to pure fluids [1], the temperature- and frequency-dependent sound velocity $c_s(t,\omega)$ and sound diffusion coefficient $D_s(t,\omega)$ are obtained by comparing the dispersion relation $\omega^2=(c_s^2+i\omega D_s)k^2$ from Eq. (3.6) with $\omega^2=(\mathcal{C}_s^2+i\omega\mathcal{D}_s)k^2$ from Eq. (3.10). From the real and imaginary parts we get

$$c_s^2(t,\omega)=\mathrm{Re}[\mathcal{C}_s^2(t,\omega)-i\omega\mathcal{D}_s(t,\omega)], \tag{3.18}$$

$$D_s(t,\omega)=-\frac{1}{\omega}\mathrm{Im}[\mathcal{C}_s^2(t,\omega)-i\omega\mathcal{D}_s(t,\omega)]. \tag{3.19}$$

These two quantities determine the experimentally observed sound attenuation $\alpha_s(t,\omega)$,

$$\alpha_s(t,\omega)=\frac{\omega^2 D_s(t,\omega)}{2c_s^3(t,\omega)}. \tag{3.20}$$

The frequency-dependent shear viscosity

$$\overline{\eta}(t,\omega)=\rho\mathcal{D}_t(t,\omega) \tag{3.21}$$

follows from Eqs. (3.7) and (3.15) and is complex at finite frequencies. The hydrodynamic transport coefficients, which concern the slow heat and diffusion mode, will be calculated at zero frequency. In this case Eqs. (3.13) and (3.14) reduce to real expressions and one may write

$$D(t)+D_c(t)=\left\{\mathrm{Tr}[\mathring{\underline{F}}_{\alpha\tilde{\alpha}}]-\frac{[\mathring{G}_{\tilde{\alpha}}]^T[\mathring{\underline{F}}_{\alpha\tilde{\alpha}}][\mathring{G}_\alpha]}{[\mathring{G}_{\tilde{\alpha}}]^T[\mathring{G}_\alpha]}\right\}_{\omega=0}, \tag{3.22}$$

$$D(t)D_c(t)=\left\{\mathring{\mathcal{F}}_{\alpha\tilde{\alpha}}\mathrm{Tr}[\mathring{\underline{F}}_{\alpha\tilde{\alpha}}]-\mathring{\Pi}_F+\frac{[\mathring{G}_{\tilde{\alpha}}]^T[\mathring{\underline{F}}_{\alpha\tilde{\alpha}}]^2[\mathring{G}_\alpha]}{[\mathring{G}_{\tilde{\alpha}}]^T[\mathring{G}_\alpha]}\right\}_{\omega=0}. \tag{3.23}$$

All equations considered so far in this section are independent of the type of critical point, which means that expressions (3.18)–(3.23) are valid at the plait point and at the consolute point. We would also like to mention that similar structures appear in other models with several secondary densities, such as $^3$He-$^4$He mixtures near the superfluid transition or magnetic liquids.

### B. Specific relations for the consolute and plait point

In order to obtain explicit expressions for the slow hydrodynamic transport coefficients, the thermal conductivity $\kappa_T$, the thermal diffusion ratio $k_T$, and the mass diffusion coefficient $D$, one needs a third equation in addition to Eqs. (3.22) and (3.23). The zeroth order of the dynamic order parameter vertex function $\mathring{f}^{(0)}_{\phi\tilde{\phi}}$ appears in the Gaussian part of the dynamic functional. From the hydrodynamic equations (3.1)–(3.3) one can derive a corresponding equation for the order parameter from the definitions (2.1)–(2.3), where the coefficient of $\nabla^2\phi_0$ appears in the Gaussian part of a corresponding ''hydrodynamic'' functional. Identifying these two Gaussian parts leads to the third equation. This identification can be extended to any order of perturbation expansion since the critical asymptotic behavior of the hydrodynamic transport coefficients and the thermodynamic derivatives appearing in the relation reproduce the correct asymptotic behavior of the vertex function. As the order parameter corresponds to different densities at the plait point and at the consolute

point, respectively, the order parameter vertex function is related to different expressions in the hydrodynamic transport coefficients. At the plait point the relation reads

$$\left(\frac{\partial\sigma}{\partial T}\right)_{c,P} D_T(t)+\left(\frac{\partial\Delta}{\partial c}\right)_{T,P} D(t)\left[\frac{k_T(t)}{T}+\left(\frac{\partial c}{\partial T}\right)_{\Delta,P}\right]^2 = \left(\frac{\partial\sigma}{\partial T}\right)_{\Delta,P} \mathring{f}_{\phi\tilde{\phi}}|_{\omega=0}, \tag{3.24}$$

while at the consolute point one simply has

$$D(t)=\mathring{f}_{\phi\tilde{\phi}}|_{\omega=0}. \tag{3.25}$$

From Eqs. (3.22), (3.23), and (3.24), or Eq. (3.25), respectively, the temperature-dependent hydrodynamic transport coefficients can be extracted. The mass diffusion and the thermal diffusion ratio at the plait point are

$$D(t)=\left(\frac{\partial\Delta}{\partial c}\right)_{\sigma,P}\left\{\left(\frac{\partial c}{\partial\Delta}\right)_{T,P} \mathring{\mathcal{F}}_{\alpha\tilde{\alpha}}|_{\omega=0} +\left(\frac{\partial c}{\partial\sigma}\right)^2_{\Delta,P}\left(\frac{\partial\sigma}{\partial T}\right)_{\Delta,P} \mathring{f}_{\phi\tilde{\phi}}|_{\omega=0} +2\left(\frac{\partial c}{\partial\sigma}\right)_{\Delta,P}\sqrt{\left(\frac{\partial\sigma}{\partial T}\right)_{\Delta,P}\left(\frac{\partial c}{\partial\Delta}\right)_{\sigma,P} \mathring{\mathcal{W}}_{\alpha\tilde{\alpha}}|_{\omega=0}}\right\}, \tag{3.26}$$

$$\frac{k_T(t)}{T}=\frac{1}{D(t)}\left\{\left(\frac{\partial c}{\partial T}\right)_{\Delta,P} \mathring{f}_{\phi\tilde{\phi}}|_{\omega=0} +\sqrt{\left(\frac{\partial\sigma}{\partial T}\right)_{\Delta,P}\left(\frac{\partial c}{\partial\Delta}\right)_{\sigma,P} \mathring{\mathcal{W}}_{\alpha\tilde{\alpha}}|_{\omega=0}}\right\}-\left(\frac{\partial c}{\partial T}\right)_{\Delta,P}, \tag{3.27}$$

where we have introduced the combination

$$\mathring{\mathcal{W}}_{\alpha\tilde{\alpha}}=\mathring{\mathcal{F}}_{\alpha\tilde{\alpha}}(\mathring{f}_{\phi\tilde{\phi}}-\mathrm{Tr}[\mathring{\underline{F}}_{\alpha\tilde{\alpha}}])+\mathring{\Pi}_F-\frac{[\mathring{G}_{\tilde{\alpha}}]^T[\mathring{\underline{F}}_{\alpha\tilde{\alpha}}]^2[\mathring{G}_{\alpha}]}{[\mathring{G}_{\tilde{\alpha}}]^T[\mathring{G}_{\alpha}]}. \tag{3.28}$$

At the consolute point the thermal diffusion ratio is given by

$$\frac{k_T(t)}{T}=\frac{1}{D(t)}\sqrt{\left(\frac{\partial\sigma}{\partial T}\right)_{c,P}\left(\frac{\partial c}{\partial\Delta}\right)_{T,P} \mathring{\mathcal{W}}_{\alpha\tilde{\alpha}}|_{\omega=0}}. \tag{3.29}$$

The expression for the thermal conductivity, which follows immediately from Eq. (3.23), is the same for both the plait point and the consolute point. We get

$$\frac{\kappa_T(t)}{\rho T}=\frac{1}{D(t)}[\mathring{\mathcal{F}}_{\alpha\tilde{\alpha}}|_{\omega=0}\mathring{f}_{\phi\tilde{\phi}}|_{\omega=0}-\mathring{\mathcal{W}}_{\alpha\tilde{\alpha}}|_{\omega=0}]. \tag{3.30}$$

We note that the expressions for the hydrodynamic coefficients (3.26), (3.27), and (3.30) for the plait point or (3.25), (3.29), and (3.30) for the consolute point are the same for both the static functional (2.4) with the secondary densities $q$ and the transformed functional (2.31) with the secondary densities $m$. The same property holds for the sound velocity (3.18) and the sound diffusion coefficient (3.19). The reason for this is that all terms appearing in Eqs. (3.11)–(3.15), from which the transport coefficients have been calculated, are invariant under the transformation (2.29).

### C. Critical sound velocity and sound attenuation

In order to decouple the fast sound mode from the slow heat and mass diffusion modes the dynamical model will be considered in the limit $\mathring{c}\to\infty$ [Eq. (2.19)]. This limit ensures that the sound mode is no critical mode. Otherwise the dynamical model could not be renormalized. In the limit $\mathring{c}\to\infty$ the explicit appearance of vertex functions in the transport coefficients differs depending on the secondary densities used. Explicit expressions for both cases are presented in Appendix C. Inserting expressions (C7)–(C10) into Eqs. (C3) and (C4), the complex functions $\mathcal{C}_s^2$ and $\mathcal{D}_s$ simplify to

$$\mathcal{C}_s^2(t,\omega)=a_j[a_1\mathring{c}_1^2+\mathring{c}_2^2\mathring{\Gamma}_{m_2m_2}(\omega)], \tag{3.31}$$

$$\mathcal{D}_s^2(t,\omega)=\mathring{f}_{l\tilde{l}}(\omega)+\frac{a_1^2\mathring{c}_1^2\mathring{\bar{\mu}}+2a_1\mathring{c}_1\mathring{c}_2\mathring{\Gamma}_{m_2m_2}(\omega)\mathring{\hat{L}}+\mathring{c}_2^2\mathring{\Gamma}^2_{m_2m_2}(\omega)\mathring{\hat{\lambda}}}{a_1\mathring{c}_1^2+\mathring{c}_2^2\mathring{\Gamma}_{m_2m_2}(\omega)}. \tag{3.32}$$

The perturbation theory only contributes to the functions $\mathring{f}_{l\tilde{l}}(\omega)$ and $\mathring{\Gamma}_{m_2m_2}(\omega)$. At zero frequency the vertex function $\mathring{\Gamma}_{m_2m_2}(\omega)$ reduces to the static vertex function introduced in Eq. (2.33) and both quantities turn into real functions. Inserting the definition of the transformed parameters, the background identification of the Onsager coefficients, and the thermodynamic expression for the static vertex function, Eqs. (3.31) and (3.32) reduce to the correct hydrodynamic coefficients

$$\lim_{\omega\to0}\mathcal{C}_s^2(t,\omega)=c_s^2(t), \quad \lim_{\omega\to0}\mathcal{D}_s(t,\omega)=D_s(t), \tag{3.33}$$

where $c_s^2$ and $D_s$ have been given in Eqs. (3.8) and (3.9). The thermodynamic expressions at the plait point as well as the corresponding expressions at the consolute point lead to the same result.

So far we have expressed the hydrodynamic transport coefficients and the sound velocity and sound diffusion by unrenormalized vertex functions of the dynamical model.

These contain singularities that have to be removed by renormalization. Expressing the unrenormalized quantities by renormalized ones, the critical temperature dependence is obtained. The procedure is equal to the pure fluid case. However, the static functional for mixtures (2.31) contains an additional density $\mathring{m}_1$. It appears only in Gaussian order, thus no perturbational contributions leading to new dimensional singularities contribute to the corresponding vertex functions and it does not need any new renormalization factor. Thus all static renormalization factors are the same as in pure fluids. From Eqs. (C7) and (C10) it can be seen that the dynamic perturbation theory does not contribute to the Onsager coefficients $\mathring{\mu},\mathring{L}$ and the coupling $\mathring{c}_1$ that appear in additional to the pure fluid case in the dynamics of mixtures. Also, in dynamics no new independent renormalization is needed. The whole renormalization procedure in the current model concerning $\phi_0$ and $\mathring{m}_2$ is equal to the procedure for the densities $\phi_0$ and $q_0$ in pure fluids, which has been extensively described in [1]. For this reason it will not be repeated in this context. A short summary of the definitions of the renormalization coefficients and the corresponding $\zeta$ functions is given in Appendix D (of course the notation has been accommodated to the current context).

Inserting the renormalized functions and parameters in Eqs. (3.31) and (3.32) is particularly easy since Eqs. (C3) and (C4) contain no explicit renormalization factors. Therefore, the unrenormalized vertex function may be immediately replaced by their renormalized counterparts. Because the separation of the unrenormalized vertex functions (B21) into static and dynamic parts is also valid for the renormalized counterparts, one gets

$$\mathcal{C}_s^2(t,\omega)=(\kappa l)^6 a_j[a_1 c_1^2(l)+c_2^2(l)\hat{\Gamma}_{m_2m_2}(v(t,l),\tilde{w}(l))], \tag{3.34}$$

$$\begin{aligned}\mathcal{D}_s(t,\omega)=(\kappa l)^2\hat{f}_{\tilde{l}\tilde{l}}(v(t,l),\tilde{w}(l))+\frac{(\kappa l)^8 a_j}{\mathcal{C}_s^2(t,\omega)}\,[&a_1^2c_1^2(l)\hat{\mu}(l)\\&+2a_1c_1(l)c_2(l)\\&\times\hat{\Gamma}_{m_2m_2}(v(t,l),\tilde{w}(l))\hat{L}_{12}(l)\\&+c_2^2(l)\hat{\Gamma}^2_{m_2m_2}(v(t,l),\tilde{w}(l))\hat{\lambda}(l)].\end{aligned} \tag{3.35}$$

$\kappa$ is a reference wave number that is usually identified by $\kappa=\xi_0^{-1}$, where $\xi_0$ is the critical correlation length amplitude. The parameters $v$ and $\tilde{w}$ are analogously defined as in the case of pure liquids,

$$v(t,l)=\frac{\xi^{-2}(t)}{(\kappa l)^2},\quad \tilde{w}(l)=\frac{\omega}{2\Gamma(l)[1-w_3^2(l)](\kappa l)^4}. \tag{3.36}$$

The parameter $\tilde{w}$ now contains an additional time scale ratio $w_3$. It is defined as

$$w_3^2(l)=\frac{\hat{L}^2(l)}{\Gamma(l)\hat{\mu}(l)}. \tag{3.37}$$

From the flow equations given in Eq. (D19) we can immediately write

$$\hat{\mu}(l)=(\kappa l)^{-2}\mathring{\mu},$$

$$\hat{L}(l)=(\kappa l)^{-1}\mathring{L}Z_\phi^{-1/2}\exp\left(\frac{1}{2}\int_1^l\frac{dx}{x}\,\zeta_\phi\right). \tag{3.38}$$

The solution of Eq. (D16) for the order parameter Onsager coefficient can be separated into a static and a dynamic part. We can write

$$\Gamma(l)=Z_\phi^{-1}\exp\left(\int_1^l\frac{dx}{x}\,\zeta_\phi\right)\Gamma^{(d)}(l), \tag{3.39}$$

where $\Gamma^{(d)}(l)$ satisfies the equation

$$l\,\frac{d\Gamma^{(d)}}{dl}=\Gamma^{(d)}\zeta_\Gamma^{(d)},\quad \Gamma^{(d)}(1)=(Z_\Gamma^{(d)})^{-1}\mathring{\Gamma}. \tag{3.40}$$

Inserting Eqs. (3.38) and (3.39) into Eq. (3.37), the time scale ratio can be rewritten as

$$w_3^2(l)=\frac{\mathring{L}^2}{\Gamma^{(d)}(l)\mathring{\mu}}. \tag{3.41}$$

From Eqs. (D14), (D19), (D15), and (D20) the renormalized couplings $c_1(l)$ and $c_2(l)$ read

$$c_1^2(l)=(\kappa l)^{-6}\mathring{c}_1^2,$$

$$c_2^2(l)=(\kappa l)^{-6}\mathring{c}_2^2Z_{m_2}^{-1}\exp\left(\int_1^l\frac{dx}{x}\,\zeta_{m_2}\right). \tag{3.42}$$

The renormalized Onsager coefficients appearing in Eqs. (3.34) and (3.35) can be obtained analogously from Eqs. (D14), (D19), (D12), and (D16). One gets

$$\hat{\lambda}(l)=(\kappa l)^{-2}\mathring{\lambda}Z_{m_2}^{-1}\exp\left(\int_1^l\frac{dx}{x}\,\zeta_{m_2}\right), \tag{3.43}$$

$$\hat{L}_{12}(l)=(\kappa l)^{-2}\mathring{L}_{12}Z_{m_2}^{-1/2}\exp\left(\frac{1}{2}\int_1^l\frac{dx}{x}\,\zeta_{m_2}\right). \tag{3.44}$$

The amplitude function $\hat{\Gamma}_{m_2m_2}(v(l),\tilde{w}(l))$ in Eqs. (3.34) and (3.35) has the general structure

$$\hat{\Gamma}_{m_2m_2}(v(l),\tilde{w}(l))=a_2[1-\gamma^2(l)G_+(v(l),\tilde{w}(l))] \tag{3.45}$$

and reduces in the zero-frequency limit to

$$\begin{aligned}\lim_{\omega\to0}\hat{\Gamma}_{m_2m_2}(v(l),\tilde{w}(l))&=\hat{\Gamma}^{(s)}_{m_2m_2}(\gamma^2(l),u(l))\\&=a_2[1-\gamma^2(l)G_+^{(s)}(\gamma^2(l),u(l))],\end{aligned} \tag{3.46}$$

where $\hat{\Gamma}^{(s)}_{m_2m_2}$ is the corresponding static function. The functions $G_+$ and $G_+^{(s)}$, respectively, accumulate the contributions of the perturbation expansion. The static coupling $\gamma_m$ always enters with $a_2$ as a reduced coupling

$$\gamma^2=\frac{\gamma_m^2}{a_2}, \tag{3.47}$$

which will be used in the following. The functions $G_+$ is related to the function $F_+$ by

$$G_+(v(l),\tilde{w}(l))=\frac{F_+(v(l),\tilde{w}(l))}{1+\gamma^2(l)F_+(v(l),\tilde{w}(l))}, \tag{3.48}$$

which is the amplitude function of the corresponding correlation function. The dynamic vertex function $\Gamma_{m_2m_2}(v(l),\tilde{w}(l))$ can then be expressed by $F_+(v(l),\tilde{w}(l))$ analogously to the static case [see Eq. (D9)]

$$\hat{\Gamma}_{m_2m_2}(v(l),\tilde{w}(l))=\frac{a_2}{1+\gamma^2(l)F_+(v(l),\tilde{w}(l))}. \tag{3.49}$$

The $Z$ factor and the exponential function in Eqs. (3.42)–(3.44) can be replaced by static functions. From Eq. (D8) we get

$$Z_{m_2}^{-1}\exp\left(\int_1^l\frac{dx}{x}\,\zeta_{m_2}\right)=\frac{\mathring{\Gamma}^{(s)}_{m_2m_2}(\xi^{-2},\mathring{\gamma}^2,\mathring{u})}{\hat{\Gamma}^{(s)}_{m_2m_2}(\gamma^2(l),u(l))}. \tag{3.50}$$

Because the unrenormalized static vertex functions are related to thermodynamics, which is shown in Appendix A, they may be replaced by thermodynamic derivatives. The amplitude function in the denominator of Eq. (3.50) has to be calculated in perturbation expansion. Inserting the relations (3.42)–(3.50) into Eqs. (3.34) and (3.35) we get

$$\mathcal{C}_s^2(t,\omega)=a_j[a_1\mathring{c}_1^2+\mathring{c}_2^2\mathring{\Gamma}^{(s)}_{m_2m_2}\mathcal{V}_s(v(l),\tilde{w}(l))], \tag{3.51}$$

$$\begin{aligned}\mathcal{D}_s(t,\omega)=&(\kappa l)^2\hat{f}_{l\tilde{l}}(v(l),\tilde{w}(l))\\&+\frac{a_j}{\mathcal{C}_s^2(t,\omega)}\{a_1^2\mathring{c}_1^2\mathring{\hat{\mu}}+2a_1\mathring{c}_1\mathring{c}_2\mathring{\Gamma}^{(s)}_{m_2m_2}\\&\times\mathcal{V}_s(v(l),\tilde{w}(l))\mathring{\hat{L}}_{12}\\&+\mathring{c}_2^2[\mathring{\Gamma}^{(s)}_{m_2m_2}\mathcal{V}_s(v(l),\tilde{w}(l))]^2\mathring{\hat{\lambda}}\}.\end{aligned} \tag{3.52}$$

In order to shorten the notation we have introduced

$$\mathcal{V}_s(v(l),\tilde{w}(l))=\frac{1+\gamma^2(l)F_+^{(s)}(u(l))}{1+\gamma^2(l)F_+(v(l),\tilde{w}(l))}. \tag{3.53}$$

The first part on the right-hand side in Eq. (3.52) describes the contribution of viscosities to the sound attenuation. The dynamic amplitude function of the longitudinal momentum density is

$$\hat{f}_{l\tilde{l}}(v(l),\tilde{w}(l))=a_j\lambda_l(l)[1+E_l(v(l),\tilde{w}(l))]. \tag{3.54}$$

The function $E_l$ collects the contributions due to perturbation expansion. From the flow equation (D18) follows the solution

$$\lambda_l=(\kappa l)^{-2}\mathring{\lambda}_l Z_{\lambda_l}^{-1}\exp\left(\int_1^l\frac{dx}{x}\,\zeta_{\lambda_l}\right) \tag{3.55}$$

for the Onsager coefficient $\lambda_l$.

The theoretical expressions for the sound velocity and the sound attenuation are obtained by inserting Eqs. (3.51) and (3.52) into Eqs. (3.18) and (3.19). The last step remaining is the specification of a relation known as the ''matching condition,'' which connects the flow parameter l with the reduced temperature $t$ and frequency $\omega$. Functions of l turn into functions of $t$ and $\omega$. The relation will be chosen in such a way as to guarantee finite-amplitude functions in the critical limits $t\to0$ and $\omega\to0$. A further condition is that the relation reduces to the well known static matching condition

$$\frac{\xi^{-2}(t)}{(\kappa l)^2}=1 \tag{3.56}$$

in the limit $\omega\to0$. Because the structure of the perturbation expansion is the same as in pure fluids, we can choose the matching condition at finite frequencies

$$\left|\left(\frac{\xi^{-2}(t)}{2(\kappa l)^2}\right)^2+i\tilde{w}(l)\right|=\frac{1}{4}. \tag{3.57}$$

The only difference from the corresponding relation in pure fluids [1] is the appearance of $\tilde{w}$, which includes the additional time scale ratio $w_3$, instead of $w$. Of course this matching condition coincides with the relation (3.56) at zero frequency as discussed before. Inserting the definition (3.36) into Eq. (3.57) we get

$$\xi^{-8}(t)+\left(\frac{2\omega}{\Gamma(l)[1-w_3^2(l)]}\right)^2=(\xi_0^{-1}l)^8. \tag{3.58}$$

In Eq. (3.58) we have also inserted the standard identification for the reference wave number $\kappa=\xi_0^{-1}$. Equation (3.58) represents an implicit equation for the flow parameter $l=l(t,\omega)$. The critical limit $t\to0$, which implies $\xi^{-1}(t)\to0$, corresponds now to a finite flow parameter value $l_c(\omega)$ tending to zero at vanishing frequency.

The asymptotic critical temperature behavior of the sound velocity and the sound attenuation is obtained by considering the limit $\omega\to0$ in Eqs. (3.51) and (3.52). In this limit $\mathcal{V}_s=1$ and $\mathcal{C}_s^2$ and $\mathcal{D}_s$ turn into real quantities. From Eqs. (3.18) and (3.51) we get immediately

$$c_s^2(t,\omega=0)=\mathcal{C}_s^2(t,\omega=0)=a_j[a_1\mathring{c}_1^2+\mathring{c}_2^2\mathring{\Gamma}^{(s)}_{m_2m_2}]=\left(\frac{\partial P}{\partial\rho}\right)_{\sigma,\rho}. \tag{3.59}$$

The last equality in Eq. (3.59) is obtained using the thermodynamic expression for the vertex function, which is given in Appendix A, and the definitions of the parameters at the plait point or at the consolute point, respectively. Because the thermodynamic derivative in Eq. (3.59) is finite at $T_c$ [29], the sound velocity stays finite also in the critical limit, which is in contrast to pure fluids where the sound velocity vanishes proportional to $t^{\alpha/2}$ in the asymptotic region. As the imaginary part of $\mathcal{C}_s^2$ vanishes at zero frequency the limit $\omega\to0$ has to be performed carefully in Eq. (3.19) to obtain the asymptotic critical behavior of $D_s$. We have to calculate the expression

$$D_s(t,\omega=0) = -\lim_{\omega\to 0} \frac{\mathrm{Im}[\mathcal{C}_s^2(t,\omega)]}{\omega} + \mathcal{D}_s(t,\omega=0). \tag{3.60}$$

An explicit calculation of this limit leads to

$$D_s(t,\omega=0) = \frac{a_j \mathring{c}_2^2 \mathring{\Gamma}^{(s)}_{m_2 m_2} \gamma^2(l)\,\mathrm{Re}[F'_+(0)]}{2\Gamma(l)[1-w_3^2(l)](\kappa l)^4[1+\gamma^2(l)F_+^{(s)}(u)]} + \mathcal{D}_s(t,\omega=0), \tag{3.61}$$

where we have defined

$$F'_+(0) = \lim_{\omega\to 0} \frac{\partial F_+(v(l),\tilde{w}(l))}{\partial \omega}. \tag{3.62}$$

The static vertex function $\mathring{\Gamma}^{(s)}_{m_2 m_2}$ is proportional to a thermodynamic derivative (see Appendix A), which tends to zero proportional to $t^\alpha$ in the critical regime. The flow parameter l is related to the reduced temperature by Eq. (3.57), leading to $l\sim t^\nu$ in the asymptotic region at zero frequency. Thus the asymptotic critical behavior of the Onsager coefficient $\Gamma$ follows from Eqs. (3.39) and (3.40) by inserting the fixed point values $\zeta_\phi^\star = -\eta$ and $\zeta_\Gamma^{(d)\star} = -x_\lambda$. This leads to an asymptotic behavior $\Gamma(t)\sim t^{-\nu(\eta+x_\lambda)}$. All other parameters in Eq. (3.61) stay finite at the critical temperature. The temperature behavior of the sound diffusion coefficient in the symptotic region is therefore

$$D_s(t,\omega=0)\sim t^{-z\nu+\alpha}, \quad z=4-\eta-x_\lambda, \tag{3.63}$$

which is the same as in pure fluids. The asymptotic divergence in Eq. (3.63) is completely contained in the first term of Eq. (3.61). The second term $\mathcal{D}_s(t,\omega=0)$ involves only subleading divergences. Inserting Eq. (3.63) into the experimentally observed sound attenuation introduced in Eq. (3.20), we get

$$\alpha_s(t,\omega)\sim \omega^2 t^{-z\nu+\alpha}, \tag{3.64}$$

which is now the same behavior as that of the sound diffusion coefficient. In pure fluids the behavior of the sound attenuation is $\alpha_s\sim\omega^2 t^{-z\nu-\alpha/2}$. The difference in the asymptotic behavior is caused by the different critical behavior of the sound velocity in pure fluids and mixtures.

## IV. COMPARISON WITH EXPERIMENT

### A. Shear viscosity at the plait and consolute point

From Eqs. (3.15) and (3.21) we obtain for the complex shear viscosity

$$\overline{\eta}(t,\omega) = \rho \mathring{f}_{tt}\tilde{}. \tag{4.1}$$

Because the momentum densities do not renormalize, the dynamic vertex function in Eq. (4.1) can be written as

$$\mathring{f}_{tt}\tilde{} = a_j(\kappa l)^2 \lambda_t(l)[1+E_t(l,\omega)], \tag{4.2}$$

where all contributions of the perturbation expansion are collected in the complex function $E_t$. The flow of the Onsager coefficient $\lambda_t$ is determined by the flow equation (D18). The solution of this equation is

$$\lambda_t(l) = (\kappa l)^{-2} \mathring{\lambda}_t Z_{\lambda_t}^{-1} \exp\left( \int_1^l \frac{dx}{x}\, \zeta_{\lambda_t} \right). \tag{4.3}$$

The asymptotic behavior of Eq. (4.3) is obtained by inserting the fixed point value $\zeta_{\lambda_t}^\star = -x_\eta$ leading to $\lambda_t(l)\sim l^{-x_\eta}$ in the asymptotic region. At zero frequency the shear viscosity turns into the real quantity

$$\overline{\eta}(t,\omega=0) = \frac{1}{RT}(\kappa l)^2 \lambda_t(l)[1+E_t(l,\omega=0)], \tag{4.4}$$

where $a_j = 1/RT\rho$. The real function $E_t(l,\omega=0) = E_t(f_t(l),w_3(l))$ depends on the time scale ratio introduced in Eq. (3.37) and the mode coupling parameter $f_t$, which is defined as

$$f_t^2(l) = \frac{g^2(l)}{\Gamma(l)\lambda_t(l)}. \tag{4.5}$$

At zero frequency the flow parameter is simply connected to the reduced temperature by the relation (3.56). Thus we immediately obtain with Eqs. (4.3) and (4.4) the asymptotic behavior of the shear viscosity as

$$\overline{\eta}(t,\omega=0)\sim t^{-\nu x_\eta}, \tag{4.6}$$

which is the same as in pure fluids. Differences between pure fluids and mixtures arise in the amplitude function $E_t$, which is now also a function of the time scale ratio $w_3$ (see Table X). The Onsager coefficient $\lambda_t(l)$ may be replaced by the mode coupling parameter $f_t$ and the Onsager coefficient $\Gamma$ using Eq. (4.5). The coefficient $g(l)$ is simply given by

$$g(l) = (\kappa l)^{-(1+\epsilon/2)} A_d^{1/2} \frac{RT}{\sqrt{N_A}}, \tag{4.7}$$

where we have used Eq. (D11) and the definition of $\mathring{g}$ in the text below Eq. (2.19). Inserting in Eq. (4.5), the Onsager coefficient may be written as

$$\lambda_t(l) = (\kappa l)^{-(2+\epsilon)} A_d \frac{(RT)^2}{N_A \Gamma(l) f_t^2(l)}. \tag{4.8}$$

The expression for the shear viscosity does not contain any thermodynamic derivative. The temperature behavior is determined by the flow of the dynamic parameters $\Gamma$(l), $f_t(l)$, and $w_3(l)$ and a simple l power. This makes the shear viscosity a suitable quantity for a comparison with experimental data to determine the initial values $\Gamma(l_0)$, $f_t(l_0)$, and $w_3(l_0)$ of the dynamic flow. With Eqs. (4.4) and (4.8) and $l = \xi_0 \xi^{-1}(t)$ the shear viscosity reads

$$\eta(t) = \frac{A_d RT}{N_A}\, \xi^\epsilon(t)\, \frac{1+E_t(f_t(t),w_3(t))}{\Gamma(t) f_t^2(t)}. \tag{4.9}$$

TABLE I. Experimental values of $\xi_0$ and the critical temperature and density in several mixtures. The $^3$He-$^4$He parameters are taken from [32]. The values for the aniline-cyclohexane mixture have been taken from [57] and [46].

| Value | PP $^3$He-$^4$He $X=0.8$ | $X=0.66$ | $X=0.45$[a] | CP $A$-$C$ $X_c=0.44$ |
|---|---|---|---|---|
| $\xi_0$ (cm) | $2.5\times10^{-8}$ | $2.4\times10^{-8}$ | $2.3\times10^{-8}$ | $2.45\times10^{-8}$ |
| $T_c$ (K) | 3.715 | 3.976 | 4.37 | 303.0 |
| $\rho_c$ (g/cm$^3$) | 0.04788 | 0.05228 | 0.0576 | 0.857 |

[a]At this mole fraction the values are obtained by interpolating the corresponding parameters between $X=0.66$ and $X=0$ ($^4$He).

The temperature flow of the dynamic parameters $\Gamma(t)$, $f_t(t)$, and $w_3(t)$ is obtained from the flow equations in Appendix D. Inserting the matching condition (3.56), we obtain from Eqs. (D16), (D21), and (D22)

$$\frac{d\Gamma}{dt}=-\xi^{-1}(t)\xi'(t)\Gamma(t)(\zeta_\Gamma^{(d)}+\zeta_\phi), \tag{4.10}$$

$$\frac{dw_3}{dt}=\frac{1}{2}\,\xi^{-1}(t)\xi'(t)w_3(t)\zeta_\Gamma^{(d)}, \tag{4.11}$$

$$\frac{df_t}{dt}=\frac{1}{2}\,\xi^{-1}(t)\xi'(t)f_t(t)(\epsilon+\zeta_\Gamma^{(d)}+\zeta_{\lambda_t}+\zeta_\phi). \tag{4.12}$$

$\xi'=d\xi/dt$ is the derivative of the correlation length. Equation (4.9), together with Eqs. (4.10)–(4.12), constitutes an exact expression for the shear viscosity in liquid mixtures at the plait point as well as at the consolute point. The amplitude function $E_t$ and the $\zeta$ functions may be inserted in any order of a loop expansion. Further, an explicit expression for the correlation length is necessary, which basically could be calculated also in a loop expansion as a function of the coupling $u$ within the $\phi^4$ model. However, for a comparison with experiments it is more useful to replace the theoretical correlation function by a function that includes experimental information. An obvious simple expression for the correlation length is

$$\xi(t)=\xi_b+\xi_0 t^{-\nu}, \tag{4.13}$$

with $\nu=0.63$. Equation (4.13) describes a correlation length that turns from the asymptotic behavior $\xi_0 t^{-\nu}$ near $T_c$ to a background value $\xi_b$ far away from the critical temperature. $\xi_0$ has been determined experimentally in several liquid mixtures, while in contrast no experimental information about the background values is available.

Therefore, we restrict the expression for the correlation length to the asymptotic form $\xi_b=0$ of Eq. (4.13) for subsequent calculations (see Table I for specific values). Inserting the one-loop expression of the amplitude function $E_t$ from Table X in Appendix D and the correlation function (4.13) into Eq. (4.9) we obtain

$$\eta(t)=\frac{RT\xi_0}{4\pi N_A t^{\nu}\Gamma(t)f_t^2(t)}\left(1-\frac{f_t^2(t)}{36[1-w_3^2(t)]}\right). \tag{4.14}$$

TABLE II. Initial temperature and corresponding values of the dynamic parameters found from a fit of the shear viscosity in several mixtures.

| Parameter | PP $^3$He-$^4$He $X=0.8$ | $X=0.65$ | $X=0.45$[a] | CP $A$-$C$ $X_c=0.44$ |
|---|---|---|---|---|
| $t_0$ | 0.07 | 0.07 | 0.07 | 0.03 |
| $10^{18}\Gamma(t_0)$ (cm$^4$/s) | 1.70 | 1.31 | 1.11 | 5.35 |
| $f_t(t_0)$ | 0.430 | 0.486 | 0.516 | 1.075 |
| $w_3(t_0)$ | 0.819 | 0.784 | 0.767 | 0.897 |

[a]At this mole fraction the initial values have been found from interpolated data.

This equation is written at $d=3$ ($\epsilon=1$), where we have $A_3=1/4\pi$. In this case the flow equations (4.10)–(4.12) reduce to

$$t\,\frac{d\Gamma}{dt}=-\frac{3\nu}{4}\,\Gamma(t)f_t^2(t), \tag{4.15}$$

$$t\,\frac{dw_3}{dt}=\frac{3\nu}{8}\,w_3(t)f_t^2(t), \tag{4.16}$$

$$t\,\frac{df_t}{dt}=-\frac{\nu}{2}\,f_t(t)\left(1-\frac{3}{4}\,f_t^2(t)-\frac{f_t^2(t)}{24[1-w_3^2(t)]}\right). \tag{4.17}$$

The initial values $\Gamma(t_0)$, $f_t(t_0)$, and $w_3(t_0)$ at some temperature distance $t_0$ can now be obtained fitting experimental shear viscosity data with Eq. (4.14) in a restricted temperature region as shown in Fig. 1. Since the data for $t<10^{-4}$ are affected by gravitation, these data were excluded from the fit. The resulting initial values are listed in Table II for $^3$He-$^4$He mixtures at the plait point and aniline-cyclohexane mixtures at the consolute point. In $^3$He-$^4$He mixtures no measurements of the shear viscosity at $X=0.45$ have been performed. In order to compare the results of our model with the experimentally measured sound velocity and attenuation at a mole fraction $X=0.45$ [30], we have generated a set of $\eta$ data at this mole fraction from the $X=0.65$ and $X=0$ data by interpolation. The procedure is justified by the simply shifted curves at different mole fractions. The fit result at $X=0.45$ is also shown in Fig. 1 and the corresponding initial values are listed in Table II, where one can see that the values at $X=0.45$ continue the behavior at $X=0.8$ and $X=0.65$ as a function of the mole fraction.

The flow of $\Gamma$, $f_t$, and $w_3$ in $^3$He-$^4$He mixtures for the three mole fractions is shown in Fig. 2. For comparison we have also plotted the flows for the pure fluids taken from [1].

### B. Critical sound propagation at plait points

The sound velocity and the sound attenuation are determined by Eqs. (3.51), (3.52), and (3.18)–(3.20). Analogous to pure fluids, the critical contributions due to the shear viscosity, the thermal conductivity, the mass diffusion, and the thermal diffusion ratio are small compared to the leading part

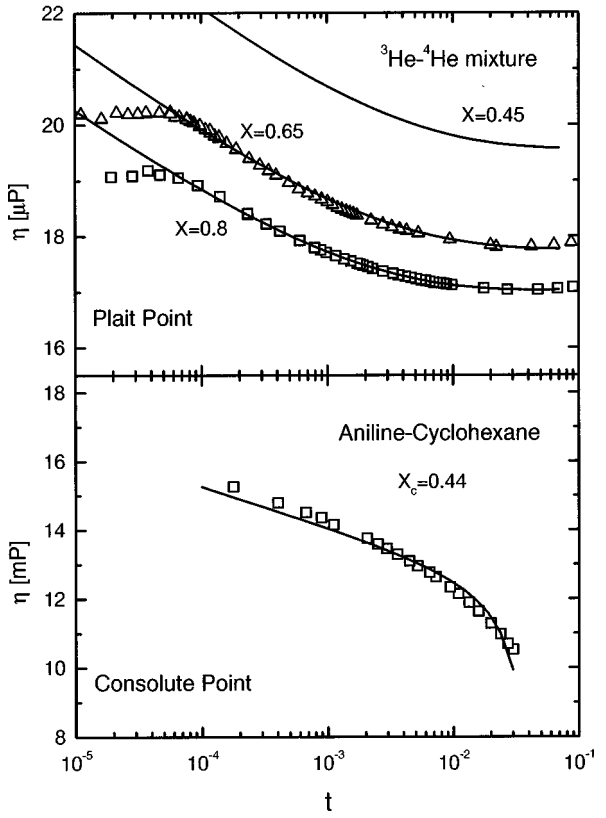


FIG. 1. Shear viscosity for $^3$He-$^4$He mixtures at the plait point and aniline-cyclohexane at the consolute point. The experimental data (squares and triangles) are taken from [58] ($^3$He-$^4$He) and [59] (aniline-cyclohexane). The fit results are represented as lines. The curve at $X=0.45$ has been found by fitting the interpolated data. The $^3$He-$^4$He data for $t<10^{-4}$ deviate from asymptotics due to gravitational effects.

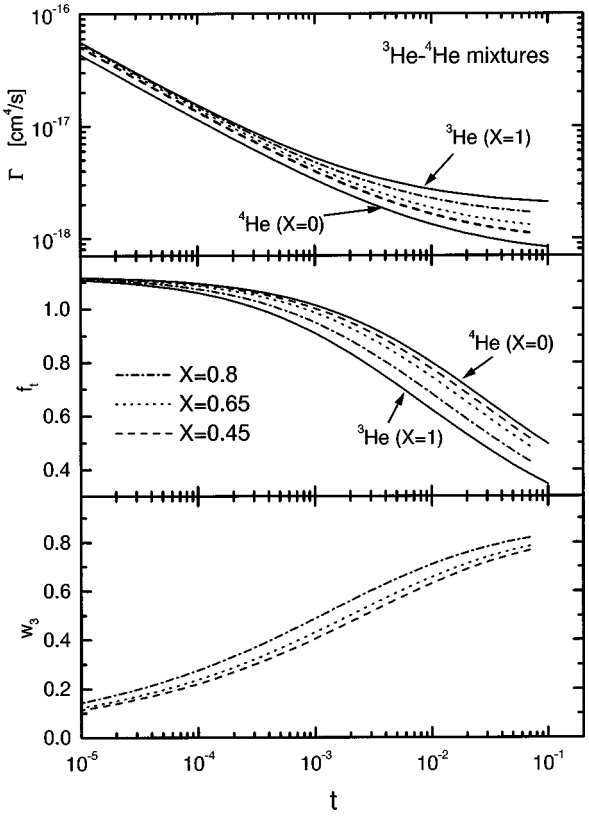


FIG. 2. Flow of the dynamical parameters found from the fit of the shear viscosity.

of the complex sound velocity $\mathcal{C}_s$. These contributions are all included in $\mathcal{D}_s$ and will be neglected in the following. In addition, this term contains a background value appearing in the sound attenuation. Therefore, the sound attenuation given in the equations below goes to zero in the background. Under these circumstances an analysis of experimental data will be performed with

$$c_s^2(t,\omega)=a_j\{a_1\mathring{c}_1^2+\mathring{c}_2^2\mathring{\Gamma}^{(s)}_{m_2m_2}\mathrm{Re}[\mathcal{V}_s(v(l),\tilde{w}(l))]\}, \tag{4.18}$$

$$D_s(t,\omega)=-\frac{1}{\omega}\,a_j\{\mathring{c}_2^2\mathring{\Gamma}^{(s)}_{m_2m_2}\mathrm{Im}[\mathcal{V}_s(v(l),\tilde{w}(l))]\}. \tag{4.19}$$

From Eq. (2.36) and the definition of the transformation matrix in Table IX it follows that the parameters $\mathring{c}_1$ and $\mathring{c}_2$ at the plait point are

$$\mathring{c}_1=\frac{RT}{\rho}\left(\frac{\partial P}{\partial\Delta}\right)_{\sigma,T_c},\quad \mathring{c}_2=\frac{RT\rho}{\chi_{\sigma,T_c}}\left(\frac{\partial c}{\partial\Delta}\right)_{\sigma,T_c}. \tag{4.20}$$

The thermodynamic expressions for the static vertex functions $a_1=\langle\mathring{m}_1\mathring{m}_1\rangle_c^{-1}$ and $\mathring{\Gamma}^{(s)}_{m_2m_2}=\langle\mathring{m}_2\mathring{m}_2\rangle_c^{-1}$ can be obtained immediately from Eqs. (A3) and (A4).

In mixtures the $T_c$ value of the sound velocity is finite because it is related to the inverse of the adiabatic compressibility at fixed concentration, which does not diverge in the limit $t\to0$. Within the model the zero-frequency sound velocity may be written as $c_s^2(t,0)=c_{sc}^2+c_b^2(t)$, where the $T_c$ value of the sound velocity is given by $c_{sc}^2=a_ja_1\mathring{c}_1^2$ and $c_b^2(t)=a_j\mathring{c}_2^2\mathring{\Gamma}^{(s)}_{m_2m_2}$. At the plait point the critical value of the sound velocity is small compared to $c_b^2(t)$ in the experimentally accessible region. This can be seen from experiments in $^3$He-$^4$He mixtures [30]. Hence we will neglect it in the following. The sound velocity at $\omega=0$ [Eq. (3.59)] can be written approximately as

$$c_s^2(t,0)=\left(\frac{\partial P}{\partial\rho}\right)_{\sigma,c}\cong c_b^2(t)=a_j\mathring{c}_2^2\mathring{\Gamma}^{(s)}_{m_2m_2}. \tag{4.21}$$

The static vertex function $\mathring{\Gamma}^{(s)}_{m_2m_2}=\langle\mathring{m}_2\mathring{m}_2\rangle_c^{-1}$ is related by Eq. (A4) to thermodynamic quantities, all of which have not been measured so far. Equation (4.21) offers the possibility to calculate the vertex function approximately from the zero-frequency sound velocity. Because the sound velocity $c_s(t,\omega)$ at finite frequency runs into $c_s(t,0)$ in the background, the background behavior of $c_s(t,\omega)$ can be used to

find a numerical expression for the zero-frequency sound velocity and the adiabatic compressibility, respectively, when measurements of $c_s(t,0)$ are not available. With Eq. (4.21) the expressions (4.18) and (4.19) may be simplified to

$$c_s^2(t,\omega)\cong\left(\frac{\partial P}{\partial\rho}\right)_{\sigma,c}\mathrm{Re}[\mathcal{V}_s(v(l),\tilde{w}(l))], \tag{4.22}$$

$$D_s(t,\omega)\cong-\frac{1}{\omega}\left(\frac{\partial P}{\partial\rho}\right)_{\sigma,c}\mathrm{Im}[\mathcal{V}_s(v(l),\tilde{w}(l))]. \tag{4.23}$$

For a numeric calculation of the complex function $\mathcal{V}_s$ defined in Eq. (3.53), it is necessary to determine the static coupling $\gamma^2(t)$. This can be done analogously to pure fluids [1] and $^4$He or $^3$He-$^4$He mixtures at the λ point [24,23] with

$$\gamma^2(t)=\frac{(2-\zeta_{\phi^2})\Delta_0^+(t)}{B_{\phi^2}-[2\zeta_{\phi^2}-\epsilon+(2-\zeta_{\phi^2})\Delta_0^+(t)]F_+^{(s)}(u)-u\zeta_u dF_+^{(s)}/du}. \tag{4.24}$$

The static functions appearing in Eq. (4.24) are defined in Appendix D. The one-loop expressions are listed in Appendix E. In addition, we have introduced the $\zeta$ function $\zeta_{\phi^2}=\zeta_r-\zeta_\phi$ in Eq. (4.24). $\Delta_0^+(t)$ is the logarithmic derivative of the $m_2$ correlation function

$$\Delta_0^+(t)=-\frac{d\ \ln\langle\mathring{m}_2\mathring{m}_2\rangle_c}{d\ \ln t}=\frac{d\ \ln\mathring{\Gamma}^{(s)}_{m_2m_2}}{d\ \ln t}. \tag{4.25}$$

With the approximation (4.21), this expression reduces to

$$\Delta_0^+(t)\cong-\frac{d\ \ln\left(\frac{\partial\rho}{\partial P}\right)_{\sigma,c}}{d\ \ln t}. \tag{4.26}$$

In $^3$He-$^4$He mixtures the sound velocity has been measured at mole fractions ($^3$He) $X=0.45$ and $X=0.8$ at 1 MHz [30]. For both mole fractions the background data (the temperature interval $0.005<t<0.1$ at $X=0.45$ and $0.003<t<0.1$ at $X=0.8$) are used to determine experimental values of $(\partial\rho/\partial P)_{\sigma,c}$, which are then fitted with the expression

$$\left(\frac{\partial\rho}{\partial P}\right)_{\sigma,c}=A_r t^{-\alpha}\frac{1+B_r t^{\Delta}}{1+(t/t_r)^{-\alpha}}, \tag{4.27}$$

with $\alpha=0.11$ and $\Delta=0.54$. With the expression (4.27) we obtain a representation of the compressibility or $c_s(t,0)$, respectively, in the experimentally accessible region. It can show a divergentlike behavior with the exponent $\alpha$ in a restricted temperature region and then, at some temperature $t_r$, it crosses over to a finite value at $t=0$. Because the background data of the sound velocity do not contain any information about the crossover temperature $t_r$, we will set $t_r=0$ in the following, which is consistent with the neglect of the critical value of the sound velocity. The fit results for the remaining parameters are listed in Table III.

TABLE III. Fit results for the adiabatic compressibility at fixed concentration at several mole fractions.

| Parameter | $X=0.45$ | $X=0.66$ | $X=0.8$ |
|---|---|---|---|
| $A_r\left(\frac{g}{\mathrm{cm}^3\ \mathrm{Torr}}\right)$ | $1.10\times10^{-5}$ | $1.17\times10^{-5}$ | $1.22\times10^{-5}$ |
| $B_r$ | $-0.653$ | $-0.617$ | $-0.592$ |

The background data calculated from the zero-frequency sound velocity and the corresponding fit curves are shown in Fig. 3. The curve at $X=0.65$ is obtained from ''data'' that have been calculated by interpolation of the sound velocity between $X=0.45$ and $X=0.8$. As stated also in Sec. IV A, the reason for this step is that the shear viscosity from which the initial values of the dynamic parameters are determined has only been measured at $X=0.65$ and $X=0.8$. Analogously to the shear viscosity, a concentration variation mainly

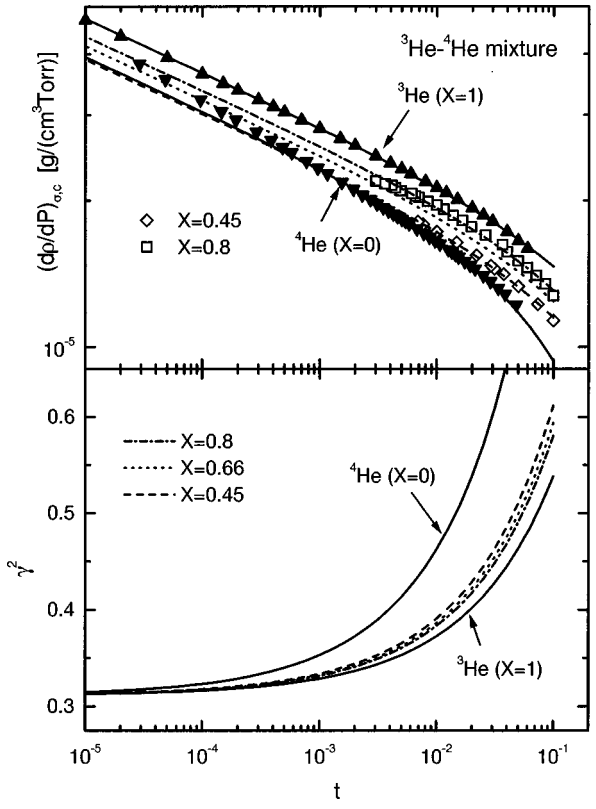


FIG. 3. Fits of the adiabatic compressibility at fixed concentration. The squares and triangles are calculated from the measured sound velocity in the background [30]. The fit results are represented by the lines. The $X=0.66$ curve is obtained by fitting the interpolated data. The static couplings $\gamma^2(t)$ at different mole fractions have been calculated from Eq. (4.24). For $\Delta_0(t)$ defined in Eq. (4.25) the fits of the adiabatic compressibility have been used.

causes a parallel shift of the sound velocity curves, while the structure of the curves nearly remains unchanged, as can be seen in [30]. The static coupling $\gamma^2(t)$ obtained with expressions (4.24) and (4.25) is plotted in Fig. 3 at different mole fractions. The coupling $u(t)$ is nearly a constant in the considered temperature region. Therefore, we have inserted the fixed point value $u^\star/4! = 0.0405$ in Eq. (4.24).

In Eqs. (4.22) and (4.23) the flow parameter $l = l(t,\omega)$ is determined by the matching condition (3.58) as a function of the reduced temperature and frequency. At each fixed frequency Eq. (3.58) defines a flow parameter $l(\bar{t})$ corresponding to an effective reduced temperature $\bar{t}$ if this value of l is inserted into the static matching condition (3.56). Thus, at $\omega = 0$, $\bar{t} = t$. A certain value of the flow parameter corresponds to different effective reduced temperatures depending on the frequency. In other words, Eq. (3.58) connects the temperature scale at $\omega = 0$, at which all functions are known from experiments to a temperature scale at finite frequency. Equation (3.58) can be rewritten as

$$\xi^{-8}(t) + \left( \frac{2\omega}{\Gamma(\bar{t})[1 - w_3^2(\bar{t})]} \right)^2 = \xi^{-8}(\bar{t}), \qquad (4.28)$$

where we have used the matching condition at zero frequency on the right-hand side. With the correlation length (4.13) ($\xi_b = 0$), the matching condition reads

$$t^8 + \left( \frac{2\omega\xi_0^4}{\Gamma(\bar{t})[1 - w_3^2(\bar{t})]} \right)^2 = \bar{t}^8. \qquad (4.29)$$

Using the solutions of the flow equations (4.15)–(4.17) with initial values found from the viscosity fits in Sec. IV A, we may now calculate for each temperature $t$ at finite frequency the corresponding reduced temperature $\bar{t}$ at $\omega = 0$ obtaining the function $\bar{t}(t,\omega)$ from Eq. (4.29). The corresponding expressions (4.22) and (4.23) turn into

$$c_s^2(t,\omega) \cong \left( \frac{\partial P}{\partial \rho} \right)_{\sigma,c} (\bar{t}) \mathrm{Re}\{\mathcal{V}_s[v(t,\bar{t}), \tilde{w}(\bar{t})]\}, \qquad (4.30)$$

$$D_s(t,\omega) \cong -\frac{1}{\omega} \left( \frac{\partial P}{\partial \rho} \right)_{\sigma,c} (\bar{t}) \mathrm{Im}\{\mathcal{V}_s[v(t,\bar{t}), \tilde{w}(\bar{t})]\}. \qquad (4.31)$$

From Eq. (3.53) we get

$$\mathcal{V}_s[v(t,\bar{t}), \tilde{w}(\bar{t})] = \frac{1 + \gamma^2(\bar{t}) F_+^{(s)} u(\bar{t})}{1 + \gamma^2(\bar{t}) F_+[v(t,\bar{t}), \tilde{w}(\bar{t})]}. \qquad (4.32)$$

Introducing the properties of the matching condition into the parameters $v$ and $\tilde{w}$ defined in Eq. (3.36), we obtain

$$v(t,\bar{t}) = \frac{\xi^{-2}(t)}{\xi^{-2}(\bar{t})}, \quad \tilde{w}(\bar{t}) = \frac{\omega\xi^4(\bar{t})}{2\Gamma(\bar{t})[1 - w_3^2(\bar{t})]}. \qquad (4.33)$$

The critical sound velocity in $^3$He-$^4$He mixtures is plotted in Fig. 4 at the mole fractions $X = 0.8$ and $X = 0.45$. The zero-frequency sound velocity has been calculated from the compressibility fits shown in Fig. 3, which also determine the static coupling $\gamma^2$. At finite frequencies no adjustable parameters remain in the sound velocity and sound attenuation. The results for the sound velocity at the frequencies $f = 1$ MHz and $f = 3$ MHz are in good agreement with the corresponding experimental data as shown in Fig. 4.

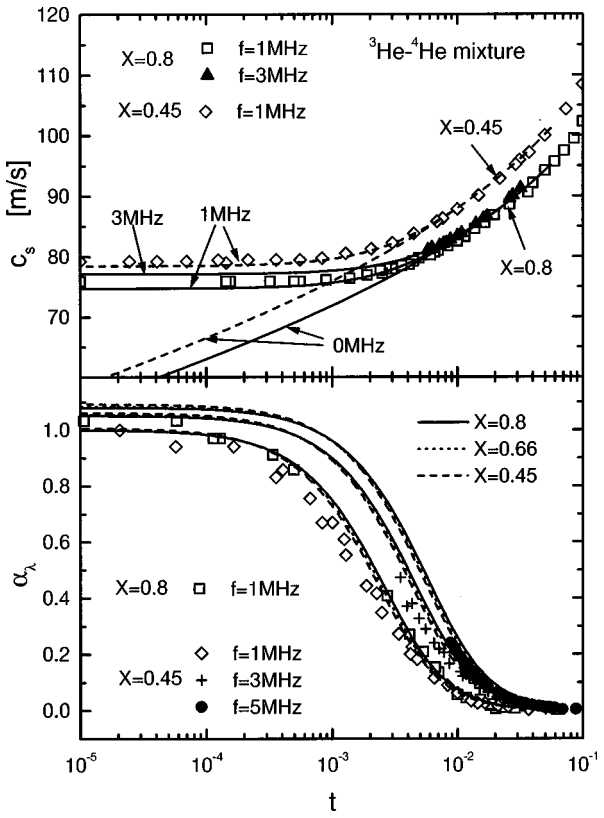


FIG. 4. Sound velocity $c_s$ and sound attenuation in one wavelength $\alpha_\lambda$ at several mole fractions and different frequencies. The 0-MHz curves for $c_s$ are determined from the experimental sound velocity data in the background. The sound velocity curves at 1 MHz and 3 MHz have been calculated without any adjustable parameter. The 1-MHz curves for $\alpha_\lambda$ are normalized to 1. The same normalization factor is used at all other frequencies. Apart from this one normalization factor, the sound attenuation curves do not include any adjustable parameter. The data have been collected from [30].

The sound attenuation in $^3$He-$^4$He mixtures at mole fraction $X = 0.8$, $X = 0.65$, and $X = 0.45$ is shown in Fig. 4. Instead of $\alpha$ defined in Eq. (3.20) we have plotted the sound attenuation in one wavelength $\alpha_\lambda = \alpha\lambda = 2\pi\alpha c_s/\omega$, which is in our theory given by

$$\alpha_\lambda(t,\omega) = -\pi \frac{\mathrm{Im}[\mathcal{C}_s^2(t,\omega)]}{\mathrm{Re}[\mathcal{C}_s^2(t,\omega)]}. \qquad (4.34)$$

Inserting the approximate expressions (4.30) and (4.31), the sound attenuation in one wavelength reads

$$\alpha_\lambda(t,\omega) \cong -\pi \frac{\gamma^2(\bar{t}) \mathrm{Im}\{F_+^*[v(t,\bar{t}), \tilde{w}(\bar{t})]\}}{1 + \gamma^2(\bar{t}) \mathrm{Re}\{F_+[v(t,\bar{t}), \tilde{w}(\bar{t})]\}}. \qquad (4.35)$$

Experimentally it has been observed that the sound attenuation in one wavelength is nearly independent from the mole

fraction [30]. This is also reproduced by the theory, as one can see in Fig. 4 at several frequencies.

### C. Critical heat and mass transport

With the same procedure that has been applied to sound in the previous sections, one can derive expressions for the heat and mass transport coefficients. With the structures in Appendix C at $\omega=0$, the thermal conductivity (3.30) turns into

$$\frac{\kappa_T(t)}{\rho T}=\frac{1}{D(t)}\left(\frac{\rho}{RT}\right)^2\left(\frac{\partial\Delta}{\partial c}\right)_{T,P}[\mathring{f}^{(d)}_{\phi\tilde{\phi}}\mathring{\mu}-\mathring{L}^2]. \quad (4.36)$$

Equations (3.31), (3.32), and (4.36) are valid for the plait point and the consolute point. The difference between the two critical points in these expressions lies in the explicit definition of the appearing model parameters. Analogously to Sec. IV B, we have to introduce the renormalized quantities to obtain functions of the reduced temperature. The only function in the above expressions that has a nontrivial dynamic renormalization is $\mathring{f}^{(d)}_{\phi\tilde{\phi}}$. The dynamic order parameter vertex function reads [the flow parameter $l(t)$ depends on $t$ via the matching condition (3.56)]

$$\mathring{f}^{(d)}_{\phi\tilde{\phi}}=Z_\phi\exp\left(-\int_1^l\frac{dx}{x}\,\zeta_\phi\right)\Gamma(l)[1+G(l)], \quad (4.37)$$

where the function $G(l)$ collects all contributions due to the perturbation expansion. Thus, with Eqs. (4.37) and (3.39) we get

$$\mathring{f}^{(d)}_{\phi\tilde{\phi}}=\Gamma^{(d)}(l)[1+G(l)]. \quad (4.38)$$

The time scale ratio $w_3$ introduced in Eqs. (3.37) and (3.41), respectively, has been defined with the transformed Onsager coefficients that correspond to the densities $\vec{m}_0$. In the above expressions the Onsager coefficients of the untransformed model appear. Analogously to Eq. (3.41), we may introduce a time scale ratio $w_3'^2(l)=\mathring{L}^2/\Gamma^{(d)}(l)\mathring{\mu}$. Inserting the transformation (2.29), one can show that both time scale ratios are equal apart from irrelevant parameters such as $\Gamma(l)/\hat{\mu}(l)\sim l^2$, which have to be neglected in the whole perturbation expansion. Thus we have $w_3'(l)=w_3(l)+O(\sqrt{\Gamma(l)/\hat{\mu}(l)})$ and it is not necessary to make a distinction between the two parameters. The l dependence in $G(l)$ enters via the model parameters. $G(l)$ generally is a function of $w_3(l)$, $f_t(l)$, and the static parameters $u(l)$ and $\gamma^2(l)$ when irrelevant parameters are neglected. Inserting Eq. (4.38) and the time scale ratio $w_3$ into Eq. (4.36), we obtain at least for the thermal conductivity the expression

$$\frac{\kappa_T(t)}{\rho T}=\frac{1}{D(t)}\left(\frac{\rho}{RT}\right)^2\left(\frac{\partial\Delta}{\partial c}\right)_{T,P}\mathring{\mu}\Gamma^{(d)}(t)[1-w_3^2(t)+G(t)]. \quad (4.39)$$

The transport coefficients are considered at zero frequency, thus the matching condition (3.56) determines the connection between the flow parameter and the reduced temperature. The fixed point value of the time ratio $w_3$ is $w_3^\star=0$, as can be seen from the flow equation in Appendix D. As a consequence, the fixed point values of the remaining parameters and the corresponding $\zeta$ functions, particularly the dynamic exponent $x_\lambda=-\zeta_\Gamma^{(d)\star}$, are the same as in pure fluids. Equation (4.39) is valid at the plait point as well as at the consolute point. However, the thermal diffusion ratio and the mass diffusion coefficient lead to different expressions for both critical points.

#### 1. Plait point

Using the general structures given in Appendix C and the thermodynamic expressions for the static vertex functions in Appendix A, the mass diffusion coefficient (3.26) and the thermal diffusion coefficient (3.27) at the plait point turn into

$$D(t)=\frac{\rho}{RT}\left(\frac{\partial\Delta}{\partial c}\right)_{T,P}\left[\mathring{\mu}+2\left(\frac{\partial c}{\partial\sigma}\right)_{\Delta,P}\mathring{L}+\left(\frac{\partial c}{\partial\sigma}\right)^2_{\Delta,P}\mathring{f}^{(d)}_{\phi\tilde{\phi}}\right], \quad (4.40)$$

$$\frac{k_T(t)}{T}=\frac{\rho}{RT}\frac{1}{D}\left[\mathring{L}+\left(\frac{\partial c}{\partial\sigma}\right)_{\Delta,P}\mathring{f}^{(d)}_{\phi\tilde{\phi}}\right]-\left(\frac{\partial c}{\partial T}\right)_{\Delta,P}. \quad (4.41)$$

Although all transport coefficients have been calculated within the transformed model represented by Eq. (2.31), in the transport coefficients (4.36)–(4.41) corresponding to the slow hydrodynamic modes, the appearing Onsager coefficients (2.34) combine in such a way that they may be replaced completely by the Onsager coefficients of the nontransformed model represented by Eqs. (2.4) and (2.18). Thus we obtain expressions for the thermal conductivity, the thermal diffusion ratio, and the mass diffusion coefficient, which are equal to those obtained in the reduced model $H'$ [3], where the effects of the fast sound mode have been neglected. This is different from the situation in $^4$He [20] and $^3$He-$^4$He mixtures [31] at the λ transition, where the sound degrees of freedom lead to small corrections to the slow hydrodynamic coefficients. Inserting Eq. (4.38) into Eqs. (4.40) and (4.41) we get the expressions

$$D(t)=\frac{\rho}{RT}\left(\frac{\partial\Delta}{\partial c}\right)_{T,P}[\mathring{\mu}+2a\mathring{L}+a^2\Gamma^{(d)}(t)[1+G(t)]], \quad (4.42)$$

$$\frac{k_T(t)}{T}=\frac{\rho}{RT}\frac{1}{D(t)}\{\mathring{L}+a\Gamma^{(d)}(t)[1+G(t)]\}-\left(\frac{\partial c}{\partial T}\right)_{\Delta,P}$$
$$=-\frac{\rho}{RT}\frac{1}{D(t)}\left[\mathring{L}+\frac{\mathring{\mu}}{a}\right]-\left(\frac{\partial c}{\partial T}\right)_{\sigma,P} \quad (4.43)$$

for the mass diffusion coefficient and the thermal diffusion coefficient. Analogously to [3], we have introduced the parameter $a$ in Eqs. (4.42) and (4.43), which is defined by

$$a=\left(\frac{\partial c}{\partial\sigma}\right)_{\Delta,P}. \quad (4.44)$$

This thermodynamic derivative is only weakly varying with the temperature and can be considered as constant in the small critical temperature region. The second equality in Eq. (4.43) has been obtained by an insertion of the explicit expression for the mass diffusion followed by a rearrangement of the appearing terms. In the first expression for $k_T$ two

strongly divergent quantities have to cancel each other by subtraction in order to obtain the correct asymptotic behavior. This shortcoming is not present in the second expression for $k_T$, which is more appropriate for numerical calculations. The asymptotic behavior of the slow transport coefficients is

$$D=D^{(c)}t^{\gamma-x_\lambda\nu},\quad k_T=k_T^{(c)}t^{-\gamma+x_\lambda\nu},\quad \kappa_T=\kappa_T^{(c)}, \tag{4.45}$$

as already shown in [3]. The connection between the coefficient $\Gamma^{(d)}(l)$ and the Onsager coefficient $\Gamma(l)$, which has been determined from the shear viscosity in Sec. IV A, has been given in Eq. (3.39). The $Z$ factor and the exponential may be eliminated with Eq. (D7). One gets

$$\Gamma(l)=\frac{\mathring{\Gamma}^{(s)}_{\phi\phi}}{(\kappa l)^2\hat{\Gamma}^{(s)}_{\phi\phi}}\,\Gamma^{(d)}(l). \tag{4.46}$$

Inserting the thermodynamic expression of the unrenormalized order parameter vertex function in Table VIII and the matching condition (3.56), the parameter $\Gamma^{(d)}$ is related to the Onsager coefficient by

$$\Gamma^{(d)}(t)=\frac{RT}{\rho}\left(\frac{\partial\sigma}{\partial T}\right)_{\Delta,P}(\xi_0^{-1}t^\nu)^2\Gamma(t). \tag{4.47}$$

In Eq. (4.47) we have replaced $\hat{\Gamma}^{(s)}_{\phi\phi}$ by its one-loop expression in Eq. (E2). In order to calculate the transport coefficients (4.39), (4.42), and (4.43) explicitly at the plait point some additional static quantities are needed from experiment. In $^3$He-$^4$He mixtures experimental information on the concentration susceptibility $(\partial X/\partial\Delta)_{T,P}$ [32], the isothermal compressibility $K_{T,X}=(1/\rho)(\partial\rho/\partial P)_{T,X}$ [33], the isochoric specific heat $C_{n,X}=T(\partial s/\partial T)_{X,n}$ [34], and $(\partial P/\partial T)_{X,n}$ [35] is available. All thermodynamic derivatives in Eqs. (4.39)–(4.47) have to be expressed by these quantities. From standard thermodynamic relation one may derive the relations

$$\left(\frac{\partial\sigma}{\partial T}\right)_{\Delta,P}=\left(\frac{\partial\sigma}{\partial T}\right)_{c,P}+\left(\frac{\partial c}{\partial T}\right)^2_{\Delta,P}\left(\frac{\partial\Delta}{\partial c}\right)_{T,P}, \tag{4.48}$$

$$\left(\frac{\partial c}{\partial T}\right)_{\Delta,P}=\frac{1}{2a}\left(\frac{\partial c}{\partial\Delta}\right)_{T,P}\left[1+\sqrt{1-4a^2\left(\frac{\partial\sigma}{\partial T}\right)_{c,P}\left(\frac{\partial\Delta}{\partial c}\right)_{T,P}}\right], \tag{4.49}$$

$$\left(\frac{\partial c}{\partial T}\right)_{\sigma,P}=\frac{1}{2a}\left(\frac{\partial c}{\partial\Delta}\right)_{T,P}\times\left[-1+\sqrt{1-4a^2\left(\frac{\partial\sigma}{\partial T}\right)_{c,P}\left(\frac{\partial\Delta}{\partial c}\right)_{T,P}}\right]. \tag{4.50}$$

The isobaric specific heat at constant concentration $(\partial\sigma/\partial T)_{c,P}$ can be expressed by the isochoric specific heat with

$$\left(\frac{\partial\sigma}{\partial T}\right)_{c,P}=\left(\frac{\partial\sigma}{\partial T}\right)_{c,\rho}+\frac{1}{\rho^2}\left(\frac{\partial P}{\partial T}\right)^2_{c,\rho}\left(\frac{\partial\rho}{\partial P}\right)_{T,c}. \tag{4.51}$$

With the above relations all static quantities apart from the unknown constant $a$ can be calculated from experimental results. In order to obtain data representations we have performed fits of several data. The concentration susceptibility has been fitted with the expression

$$\left(\frac{\partial X}{\partial\Delta}\right)_{T,P}=D_b+D_0t^{-x}, \tag{4.52}$$

with $D_b$, $D_0$, and $x$ variable parameters. For the isochoric specific heat we have taken the expression

$$C_{n,X}=A_ct^{-\alpha}(1+B_ct^\Delta). \tag{4.53}$$

The exponents $\alpha=0.11$ and $\Delta=0.54$ are fixed. An appropriate fit form for the isothermal compressibility turned out to be

$$K_{T,X}=\frac{K_xt^{-\gamma'}}{1+\left(\frac{t}{t_x}\right)^{-\gamma'}}, \tag{4.54}$$

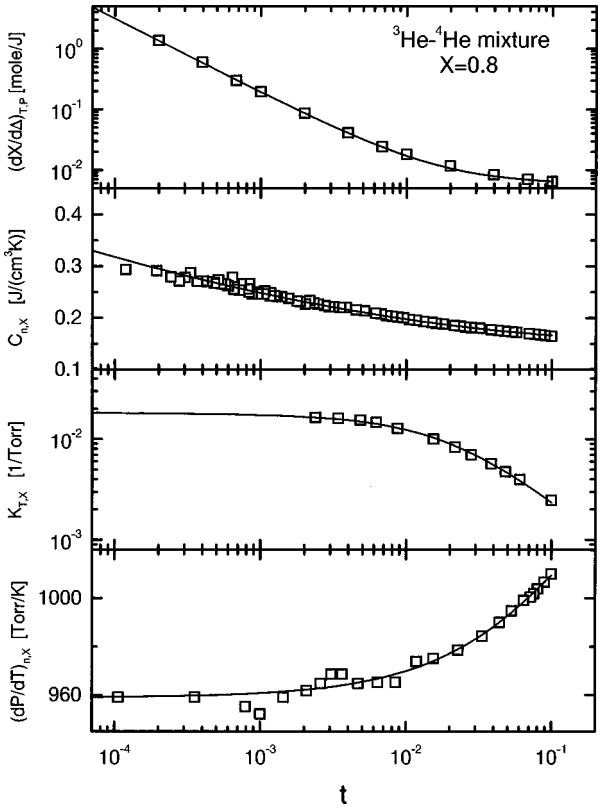


FIG. 5. Experimentally determined thermodynamic derivatives and the corresponding fits performed with Eqs. (4.52)–(4.55). The data are taken from [32] for the concentration susceptibility, the isochoric specific heat [33], the isothermal compressibility [34], and for $(\partial P/\partial T)_{n,X}$ [35].

TABLE IV. Fit results of the concentration susceptibility (4.52), the isochoric specific heat (4.53), the isothermal compressibility (4.54), and $(\partial P/\partial T)_{X,n}$ [Eq. (4.55)] in $^3$He-$^4$He mixtures at $X=0.8$.

| | |
|---|---|
| $D_b$ (mole/J) | $5.8\times10^{-3}$ |
| $D_0$ (mole/J) | $4.1\times10^{-5}$ |
| $x$ | 1.22 |
| $A_c$ (J/cm$^3$ K) | 0.115 |
| $B_c$ | 0.429 |
| $K_x$ (Torr$^{-1}$) | $1.66\times10^{-4}$ |
| $t_x$ | $2.14\times10^{-2}$ |
| $a_0$ (Torr/K) | 959 |
| $a_1$ (Torr/K) | −1363.3 |
| $a_2$ (Torr/K) | −391 |
| $B$ (Torr/K) | 1480.6 |

with a fixed effective exponent $\gamma'=1.19$, which has been used also in pure fluids [1]. At least $(\partial P/\partial T)_{X,n}$ has been fitted with the same expression used in pure fluids, which is

$$\left(\frac{\partial P}{\partial T}\right)_{X,n}=a_0+a_1t+a_2t^2+Bt^{1-\alpha}, \tag{4.55}$$

with the same exponent $\alpha$ as in Eq. (4.53). The $T_c$ value $a_0$ has been fixed at each mole fraction, while the remaining parameters $a_1$, $a_2$, and $B$ have been determined by the fit. The fit results for all quantities are listed in Table IV.

The static data and the corresponding fits are shown in Fig. 5. At this stage three constant parameters $\mathring{\mu}$, $\mathring{L}$, and $a$ remain unknown, while the initial values $\Gamma(t_0)$, $f_t(t_0)$, and $w_3(t_0)$ have been determined from a shear viscosity fit. These three parameters may be found by a fit of the thermal conductivity $\kappa_T$ and the thermal diffusion ratio $k_T$ in a small temperature region $10^{-3}\leqslant t\leqslant 10^{-2}$ where experimental data are available [36,37]. The results of the calculation are shown in Fig. 6 as solid lines. The mass diffusion coefficient $D$, which is also experimentally available at this mole fraction [38], has been calculated without any adjustable parameter and is shown in the same figure. The fit region is indicated by a bar in the $\kappa_T$ and $k_T$ plot. The obtained values for $\mathring{\mu}$, $\mathring{L}$, and $a$ are listed in the first column of Table V.

In Fig. 6 one can see a deviation of the calculated solid lines and the experimental data of $\kappa_T$ and $k_T$. This deviation may be removed by a change of the fitting procedure. Instead of calculating the flow from shear viscosity fits alone, it is also possible to perform a common fit of $\eta$, $\kappa_T$, and $k_T$ that determines all six parameters $\Gamma(t_0)$, $f_t(t_0)$, $w_3(t_0)$, $\mathring{\mu}$, $\mathring{L}$, and $a$ in one step. The result of this procedure is shown as dashed lines in Fig. 6. Now the background behavior of $\kappa_T$ and $k_T$ is better than in the previous fitting procedure, but deviations in the shear viscosity appear. Each improvement in the thermal transport coefficients causes a deviation in the shear viscosity. This background deviations imply that one or more coefficients include temperature-dependent regular background contributions that are not contained in our model. The effect of such contributions and the systematic

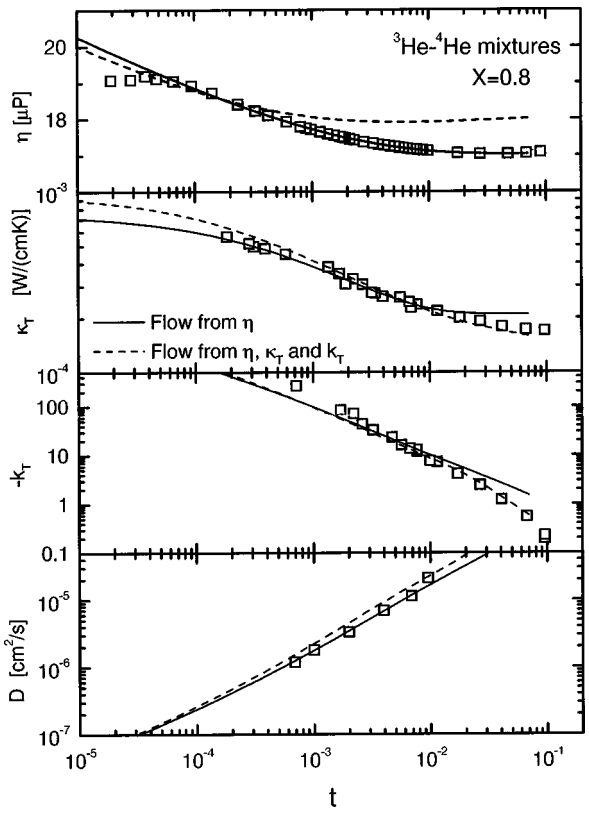


FIG. 6. Transport coefficients in $^3$He-$^4$He mixtures. $\kappa_T$ and $k_T$ have been fitted in the temperature region $10^{-3}<t<0.1$. $D$ has been calculated without any adjustable parameters. The data have been taken from [36–38].

correction procedure has recently been discussed in [13,39], where as an explicit example the shear viscosity in 2-butoxyethanol–water mixtures at the consolute point has been considered. In Fig. 7 we compare the flow obtained from the shear viscosity fits at $X=0.8$ from Fig. 2 (solid lines) with the flow obtained by fitting $\eta$, $\kappa_T$, and $k_T$ (dashed lines). In the background the Onsager coefficient $\Gamma$ obtained from the second procedure is larger than the one from the shear viscosity fit causing the deviation in the shear viscosity [dashed line in Fig. 6(a)]. The time scale ratio $w_3$ is growing with the improved background behavior of $\kappa_T$ and $k_T$, which means a decrease in $1-w_3^2$. Together with the increasing $\Gamma$, this implies that the effective Onsager coefficient $\Gamma(1-w_3^2)$ entering the matching condition is only slightly varying. The frequency-dependent kink in the sound velocity and the sound attenuation is mainly determined by this effective Onsager coefficient. As a consequence, the difference of the flows in Fig. 7 should have only a weak influence on the sound velocity and the sound attenuation. This is verified in Fig. 8, where we have compared the sound velocities and sound attenuations following from the two different flows.

#### *2. Consolute point*

The mass diffusion coefficient and the thermal diffusion ratio at the consolute point are obtained from Eqs. (3.25) and (3.29):

$$D(t)=\frac{\rho}{RT}\left(\frac{\partial\Delta}{\partial c}\right)_{T,P}\mathring{f}^{(d)}_{\phi\tilde{\phi}}, \tag{4.56}$$

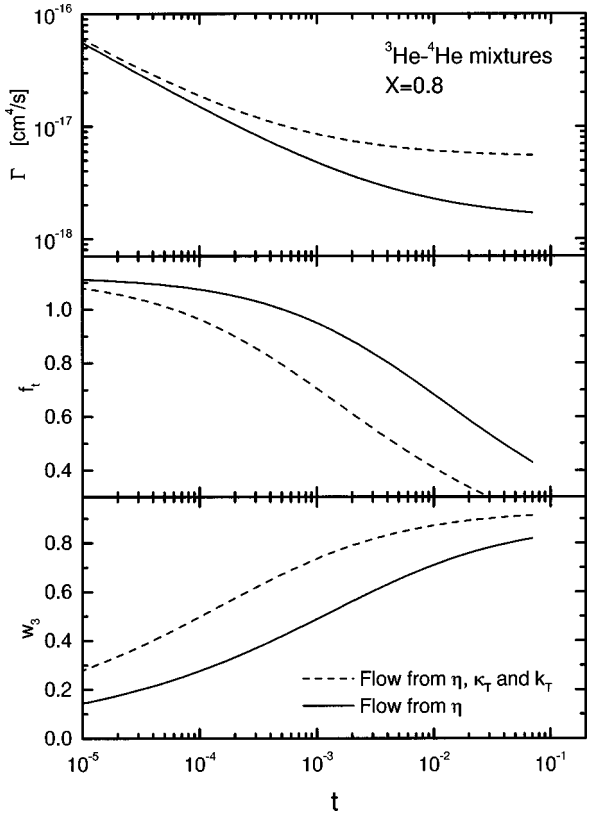


FIG. 7. Comparison of the flow of the dynamical parameters found from a fit of the shear viscosity (solid lines) with the flow found from the fit of the shear viscosity, the thermal conductivity, and the thermal diffusion ratio (dashed lines).

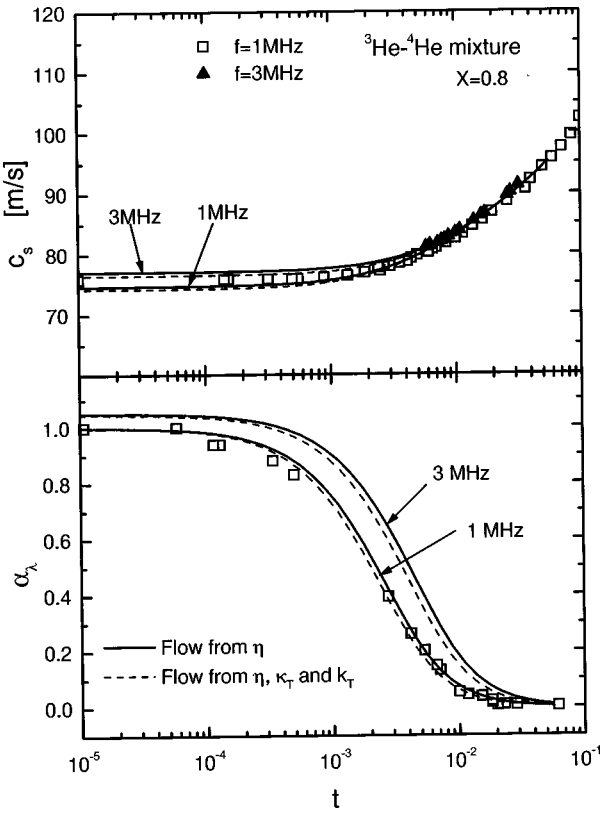


FIG. 8. Sound velocity $c_s$ and sound attenuation in one wavelength $\alpha_\lambda$ calculated from different flows. The full lines are those of Fig. 4 with the parameters found from a fit of the shear viscosity; the dashed lines are from a fit of the shear viscosity, thermal conductivity, and thermal diffusion ratio. The data have been taken from [30].

$$\frac{k_T(t)}{T}=\frac{\rho}{RT}\frac{\mathring{L}}{D(t)}. \tag{4.57}$$

Inserting Eq. (4.38) into Eq. (4.56), we get the expression

$$D(t)=\frac{\rho}{RT}\left(\frac{\partial\Delta}{\partial c}\right)_{T,P}\Gamma^{(d)}(l)[1+G(l)] \tag{4.58}$$

for the mass diffusion coefficient at the consolute point. The asymptotic behavior of the transport coefficients at the consolute point is the same as at the plait point in Sec. IV C 1. Analogously to the plait point, the coefficient $\Gamma^{(d)}$ is related by Eq. (4.46) to the Onsager coefficient $\Gamma$. However, the static order parameter vertex function now corresponds to another thermodynamic derivative, as can be seen from Table VIII. Therefore, Eq. (4.46) turns into

$$\Gamma^{(d)}(t)=\frac{RT}{\rho}\left(\frac{\partial c}{\partial\Delta}\right)_{T,P}(\xi_0^{-1}t^\nu)^2\Gamma(t) \tag{4.59}$$

at the consolute point. Inserting into Eq. (4.58) we obtain

$$D(t)=(\xi_0^{-1}t^\nu)^2\Gamma(t)[1+G(t)]. \tag{4.60}$$

The mass diffusion coefficient is completely determined by the dynamic flow, which has been found for aniline-cyclohexane mixtures from the shear viscosity in Sec. IV A. Therefore, $D$ can be calculated from Eq. (4.60) without any adjustable parameter and compared with the corresponding data in [40]. There the thermal diffusion ration has also been measured. The thermal diffusion ratio is immediately determined by Eq. (4.57) with $\mathring{L}$ as an adjustable parameter. In Fig. 9 we have compared the results for the mass diffusion coefficient and the thermal diffusion coefficient with the experimental data taken from [40]. Choosing $\mathring{L}=3.75\times10^{-5}$ J cm$^5$/g s K mole, the calculated $k_T$ curve is in good agreement with the data.

## V. COMPARISON WITH THE FERRELL-BHATTACHARJEE THEORY AT THE CONSOLUTE POINT

Most of the critical sound experiments near the consolute point have been analyzed in terms of the theory of Ferrell and Bhattacharjee (see Fig. 10). They start in their phenomenological theory from the thermodynamic expression for the adiabatic sound velocity and isolate the singular contribution related to the specific heat at constant pressure and concentration $C_{p,c}(t)$ [14]. By scaling arguments and observing the Kramers-Kronig relations they generalize the static sound

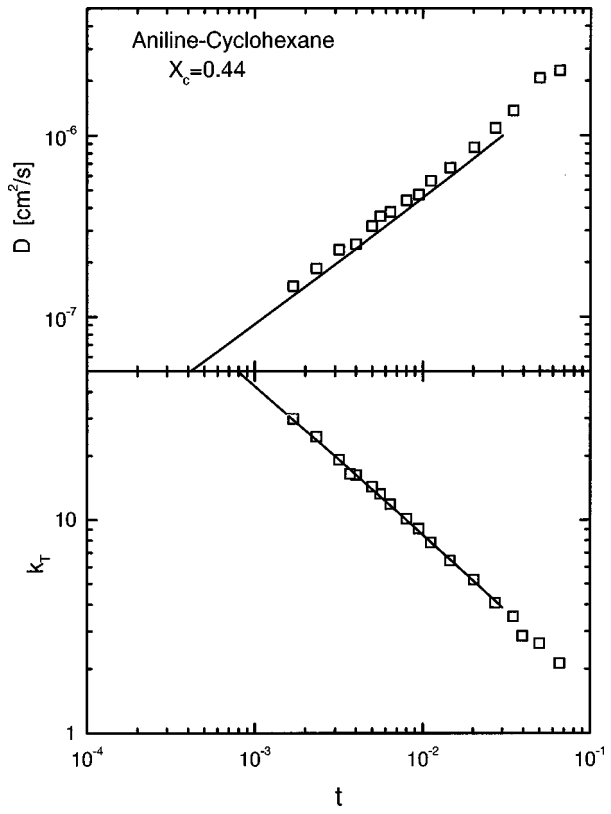


FIG. 9. Transport coefficients in aniline-cyclohexane mixtures. In $k_T$ the parameter $\mathring{L}$ has been adjusted. $D$ has been calculated without any adjustable parameters. The data have been taken from [40].

velocity to the complex frequency-dependent sound velocity, which is, in our notation, $\mathcal{C}_s(t,\omega)$, by introducing a frequency-dependent specific heat $C_{p,c}(t,\omega)$ [15,41], which is calculated within the decoupled mode theory [42].

In our theory the transformation (2.29) eliminates one of the static couplings $\gamma_i$, which leads to the separation of nonsingular and singular parts in the complex sound velocity. Physically, this means introducing variations along and perpendicular to the phase transition line $T_c(P)$. Analogously to

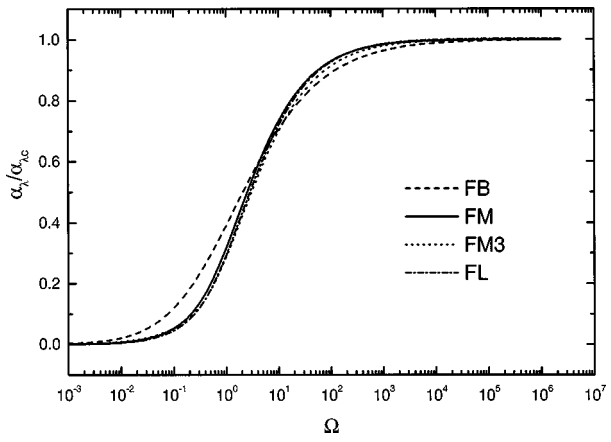


FIG. 10. Comparison with the result of Ferrell and Bhattacharjee: FB, Ferrell and Bhattacharjee's empirical function; FM, our result in the $\epsilon$ expansion; FM3, our result in $d=3$; FL, our result for pure fluids.

TABLE V. Comparison of the two fitting procedures in $^3$He-$^4$He mixtures at $X=0.8$. In the first procedure (flow from $\eta$) the initial values $\Gamma(t_0)$, $f_t(t_0)$, and $w_3(t_0)$ have been determined by a fit of the shear viscosity alone, while the constants $\mathring{\mu}$, $\mathring{L}$, and $a$ have been found by a fit of $\kappa_T$ and $k_T$. In the second procedure (flow from $\eta$, $\kappa_T$, and $k_T$), all six parameters have been found by a common fit of $\eta$, $\kappa_T$, and $k_T$.

| Parameter | Flow from $\eta$ | Flow from $\eta$, $\kappa_T$, and $k_T$ |
|---|---|---|
| $\Gamma(t_0)$ (cm$^4$/s) | $1.70\times10^{-18}$ | $5.54\times10^{-18}$ |
| $f_t(t_0)$ | 0.430 | 0.232 |
| $w_3(t_0)$ | 0.819 | 0.913 |
| $\mathring{\mu}$ (cm$^5$/s mole) | $2.19\times10^{-4}$ | $1.49\times10^{-3}$ |
| $\mathring{L}$ (cm$^{9/2}$/s$\sqrt{\text{mole}}$) | $5.40\times10^{-3}$ | $-3.52\times10^{-2}$ |
| $a$ (gK/J) | $8.89\times10^{-3}$ | $2.05\times10^{-2}$ |

the plait point considered in Sec. IV, the sound velocity and the sound attenuation are determined by the complex function $\mathcal{C}_s$ given in Eq. (3.51). Contributions from heat and mass transport included in $\mathcal{D}_s$ are negligible. The only difference from the plait point is that now the parameters $\mathring{c}_1, \mathring{c}_2$ and the static vertex functions $a_1$ and $\mathring{\Gamma}_{m_2m_2}$ correspond to other thermodynamic derivatives. From Eq. (2.36) and Table IX we get

$$\mathring{c}_1=\frac{RT}{\rho}\left(\frac{\partial P}{\partial T}\right)_{c,T_c}, \quad \mathring{c}_2=\frac{RT^2\rho}{C_{c,T_c}}\left(\frac{\partial \sigma}{\partial T}\right)_{c,T_c}. \tag{5.1}$$

The thermodynamic expressions of the static vertex functions $a_1$ and $\mathring{\Gamma}_{m_2m_2}$ are immediately obtained from Eqs. (A5) and (A6). As discussed in Sec. IV, the sound velocity at zero frequency can be written as $c_s^2(t)=c_{sc}^2+c_b^2(t)$, with $c_{sc}^2=a_j a_1 \mathring{c}_1^2$ and $c_b^2(t)=a_j \mathring{c}_2^2 \mathring{\Gamma}_{m_2m_2}$. In contrast to the plait point, the critical value $c_{sc}$ is now large compared to the fluctuation induced part $c_b(t)$. This suggests an expansion of $c_s(t)-c_{sc}$ into powers of the small ratio $c_b(t)/c_{sc}$. We rewrite the sound velocity as

$$\begin{aligned} c_s(t)-c_{sc}&=c_{sc}\left(\sqrt{1+\frac{c_b^2(t)}{c_{sc}^2}}-1\right) \\ &\simeq \frac{c_b^2(t)}{2c_{sc}}\simeq\frac{g^2}{2}\frac{c_{sc}^3}{T_c}\frac{1}{C_{P,c}(t)}, \end{aligned} \tag{5.2}$$

with a coupling constant $g$, which has been introduced by Ferrell and Bhattacharjee. Neglecting the temperature-dependent term in the denominator of $c_b^2(t)$, we obtain from our expressions [with Eqs. (2.32), (2.33), (A5), and (A6) and $a_j=1/R\rho T_c$]

$$g=\rho T_c\left(\frac{\partial \sigma}{\partial T}\right)_{c,T_c}\left(\frac{\partial T}{\partial P}\right)_{c,T_c}, \tag{5.3}$$

in agreement with Ferrell and Bhattacharjee.

The next step is to compare the frequency dependence. Since no experimental results concerning the frequency de-

pendence of the sound velocity are available, we restrict ourselves in this discussion to the frequency-dependent sound absorption. The most appropriate quantity is the sound absorbtion in one wavelength since several theoretical forms including the result of Ferrell and Bhattacharjee have been compared recently [43,44]. For this purpose we have to restrict our expressions on the one hand to the asymptotic critical region, regarding the solution of the matching condition. On the other hand, we have to remain in the nonasymptotic region concerning the dependence of the static specific heat and the coupling $\gamma$ on the frequency-dependent effective temperature. A typical temperature flow for this coupling is shown in Fig. 11. Contrary to the behavior near a plait point (see Fig. 3), $\gamma$ is a decreasing function near the consolute point. This temperature dependence is related to the nonuniversal amplitude of the Wegner correction [13]. The quantity studied is the sound absorption in one wavelength introduced in Eq. (4.34). Inserting the complete expression (3.51) into Eq. (4.34) we obtain

$$\alpha_\lambda = \pi \frac{c_b^2(\bar{t})\gamma^2(\bar{t})\mathrm{Im}[F_+(v(\bar{t}),\tilde{w}(\bar{t}))]\,\dfrac{1+\gamma^2(\bar{t})F_+^{(s)}(u(\bar{t}))}{|1+\gamma^2(\bar{t})F_+(v(\bar{t}),\tilde{w}(\bar{t}))|^2}}{c_{sc}^2 + c_b^2(\bar{t})\{1+\gamma^2(\bar{t})\mathrm{Re}[F_+(v(\bar{t}),\tilde{w}(\bar{t}))]\}\,\dfrac{1+\gamma^2(\bar{t})F_+^{(s)}(u(\bar{t}))}{|1+\gamma^2(\bar{t})F_+(v(\bar{t}),\tilde{w}(\bar{t}))|^2}}. \tag{5.4}$$

The static coupling $\gamma^2$ has to be calculated according to Eq. (3.47). The amplitude functions $F_+(v,\tilde{w})$ and $F_+^{(s)}(u)$ are listed in Appendix E in one-loop order. The temperature scale $\bar{t}=\bar{t}(t)$ follows from the matching condition (3.58). In the experimental region $\gamma^2(\bar{t})$ is smaller than its fixed point value and we may neglect the $\gamma^2$ terms against 1 (see Fig. 11). Neglecting also the second term in the denominator, the expression simplifies to

$$\alpha_\lambda = \pi \frac{c_b^2(\bar{t})\gamma^2(\bar{t})}{c_{sc}^2}\mathrm{Im}[F_+(v(\bar{t}),\tilde{w}(\bar{t}))]. \tag{5.5}$$

Dividing by the sound attenuation in one wavelength at $T_c$ we obtain the final result, which has to be compared with the empirical function given by Ferrell and Bhattacharjee,

$$\frac{\alpha_\lambda}{\alpha_{\lambda c}} = G_{FB}(\Omega) = \left[1+0.414\left(\frac{2.1}{\Omega}\right)^{1/2}\right]^{-2}, \tag{5.6}$$

where $\Omega = \omega/2\Gamma_{as}\xi_0^{-4}t^{z\nu}$ and $\Gamma_{as}$ has to be taken from the asymptotic behavior of the order parameter Onsager coefficient. Our expression reads

$$\frac{\alpha_\lambda}{\alpha_{\lambda c}} = G_{FM}(\Omega) = \frac{c_b^2(\bar{t})\gamma^2(\bar{t})}{c_b^2(\bar{t}(T_c))\gamma^2(\bar{t}(T_c))}\frac{\mathrm{Im}[F_+(v(\bar{t}),\tilde{w}(\bar{t}))]}{\pi/16}. \tag{5.7}$$

Note that the matching condition has to be solved in the asymptotic regime. This leads to the scaling solution [1]

$$\bar{t}^\nu = t^\nu S(\Omega), \tag{5.8}$$

with $S$ being the solution of $S^8 = 1+16\Omega^2 S^{2(4-z)}$. As a further approximation (used by Ferrell and Bhattacharjee) that is valid in the experimental regime we take $c_b^2$ as constant and $\gamma^2(\bar{t}) \simeq \mathrm{const}\times t^\alpha$. Then $G_{FM}$ reads

$$G_{FM}(\Omega) = \left(\frac{\bar{t}}{\bar{t}(T_c)}\right)^\alpha \frac{\mathrm{Im}[F_+(v(\bar{t}),\tilde{w}(\bar{t}))]}{\pi/16}. \tag{5.9}$$

It is obvious that for large $\Omega$ both functions reach the value $G=1$, whereas for small $\Omega$ they reach the value $G=0$. However, the approach to zero is different: $G_{FB}\sim\Omega$, whereas $G_{FM}\sim\Omega^{1-\alpha/z\nu}$. This is a small effect mentioned but neglected by Ferrell and Bhattacharjee. If we do the same we may simply write

$$G_{FM}(\Omega) = \frac{\mathrm{Im}[F_+(v(\bar{t}),\tilde{w}(\bar{t}))]}{\pi/16}, \tag{5.10}$$

shown in Fig. 10 and compared with other calculations. It is also of interest to compare $\alpha_\lambda/\alpha_{\lambda c}$ with the result valid for pure fluids. There we have $c_{sc}=0$ and

$$\alpha_\lambda = \pi \frac{\gamma^2(\bar{t})\mathrm{Im}[F_+(v(\bar{t}),\tilde{w}(\bar{t}))]}{1+\gamma^2(\bar{t})\mathrm{Re}[F_+(v(\bar{t}),\tilde{w}(\bar{t}))]}. \tag{5.11}$$

If we take for the static coupling $\gamma^2$ its fixed point value, we find for the ratio

$$\frac{\alpha_\lambda}{\alpha_{\lambda c}} = G_{FM}(\Omega)\,\frac{1+0.35\ \mathrm{Re}[F_+(v(\bar{t}(T_c)),\tilde{w}(\bar{t}(T_c)))]}{1.06}. \tag{5.12}$$

Neglecting the factor of $G_{FM}(\Omega)$, we can conclude that under the conditions mentioned the ratio of sound absorption in the mixtures and the pure fluid scale with the same universal scaling function. Thus we have derived, on the basis of the stochastic models describing the respective critical dynamics, what has been observed within the phenomenological theory [45]. There an effective, nonasymptotic scaling frequency has been introduced, quite similar to Eq. (6.5) in [1].

However, we want to remark that the asymptotic properties of the sound attenuation in mixtures and pure fluids are different. For example, whereas for pure fluids at $T_c$, $\alpha_\lambda$ goes to a constant for $\omega\to 0$ in mixtures, it goes to zero like $\alpha_\lambda\sim\omega^{\alpha/z\nu}$. Only in the experimentally observable region is the ''universality'' of the ratio considered above established by the validity of the approximation made. Universality in fluids and mixtures is based on the renormalization properties, namely, the fact that all renormalizations necessary can be expressed by those of model $H$. There are other nonuni-

versal properties; for a striking example see the enhancement of the thermal conductivity near the consolute point, which is governed by the parameter $w$ present only in the extended model $H'$ [13]. We would like to note that in a mixture there are *two* dynamic exponents of transient correction to scaling: One corresponds to the mode coupling and has the same value as in pure fluids $\omega_f = \epsilon$ and the other one corresponds to the parameter $w$ present only in mixtures and is related to the pure fluid exponent $x_\lambda$ of the thermal conductivity $\omega_w = x_\lambda/2 \sim \epsilon/2$.

## VI. CONCLUSION

We have presented a nonasymptotic renormalization group theory for the critical behavior of the hydrodynamic modes including the sound mode. Nonuniversal parameters enter the theory. These are background values of the model Onsager coefficients, $\Gamma_0$ (the renormalized coefficient for the order parameter), the unrenormalized values $\mathring{\mu}$ and $\mathring{L}$, the renormalized ratio of Onsager coefficients $w_3(t_0)$, and the mode coupling constant $f(t_0)$. The static quantities are taken directly from experiments and/or are calculated from measured quantities using thermodynamic relations. The dynamic field theoretic functions are calculated within the one-loop approximation. Within this approximation the asymptotic critical exponent for the shear viscosity is given by $x_\eta = 1/19 = 0.053$ [2] and the asymptotic value of the Kawasaki amplitude by $R = 1.056$ [12]. Whereas the Kawasaki amplitude agrees with the value adopted in mode coupling theory [5] and found in the asymptotic region [46], the critical exponent $x_\eta$ seems to be too small. Theoretical calculations beyond one-loop order lead to values between 0.04 [47] up to 0.068 [48], whereas experimental values in the region $0.067 \pm 0.003$ [49] were found. One may treat the exponent $x_\eta$ as a parameter keeping the correct value of the asymptotic Kawasaki amplitude [50] and improve the fit as well as the predictions. However, this has to include gravitational effects besides the background effects, at least near the gas-liquid phase transition extending the calculation to noncritical values of the density. This has been done for pure fluids in [50] and qualitatively similar agreement with experiment could be reached as in mode coupling theory [5]. We expect this be the case also for mixtures.

The situation concerning the transport coefficients of $^3$He-$^4$He mixtures is not completely satisfying; improvements of the fits of the thermal conductivity and of the thermal diffusion ratio are at the expense of the agreement with the shear viscosity. We attribute this to uncertainties in the static quantities used in the background. So far consistency of the data for the transport coefficients can be checked only within 10%. We would like to mention that only for $^3$He-$^4$He mixtures are we in the favorable situation of having experimental values available for all three transport coefficients and the sound mode. For other mixtures near the gas-liquid critical point only the thermal conductivity could be compared with mode coupling calculations (for $CO_2$-ethane mixtures see [5]; for methane-ethane mixtures see [51]).

Concerning mixtures near the consolute point it would be worthwhile to look for examples other than 2-butoxyethanol–water mixtures, where a measurable enhancement of the thermal conductivity is observed. Furthermore, it would be of interest to extend the verification of the exact relation between the mass diffusion $D$ and the thermal diffusion ratio $k_T$, $D/k_T = \text{const}$, further out to the background.

Another point of interest is the temperature dependence of the correlation length, which enters the matching condition. The crossover of the correlation length to its background value is of importance and favorable conditions in light scattering experiments may be found in binary polymeric mixtures [52,53]. The consequences of a possible crossover to ''mean field theory'' on the behavior of the dynamical quantities [54] should be worked out. The small critical exponent found in polymer solutions, $x_\eta = 0.044$, [55] is so far unexplained and connected with the question of another universality class for these systems.

Regarding the sound propagation near the consolute and the gas-liquid critical point the theory can be extended to noncritical concentrations and densities, respectively. For the first case data are available for aniline-cyclohexane mixtures [44].

## ACKNOWLEDGMENTS

We thank H. Meyer for sending us experimental data; we also acknowledge useful discussions with J. Luettmer-Strathmann and H. Meyer. This work was supported by the Fonds zur Förderung der wissenschaftlichen Forschung under Project No. P12422-TPH.

## APPENDIX A: EXPLICIT EXPRESSIONS FOR STATIC QUANTITIES

In this appendix we give some connections between the quantities defined in the theoretical model and thermodynamics. Clearly, these connections depend on the critical point (plait or consolute point) one considers. The coefficients of the matrix $\overleftrightarrow{A}$ in the static functional (2.4) represent the second-order expansion coefficients in an expansion of the internal energy in powers of the extensive densities [3]. Therefore, they are determined by second-order derivatives of the internal energy in the thermodynamic background, which are equal to first-order derivatives of the intensive fields. The coefficients have been summarized in Table VI for both critical points.

The superscript (0) indicates background values, which are considered as constants in the critical region. The coefficients of the matrix $\overleftrightarrow{A}$ and the couplings $\mathring{\vec{\gamma}}_q$ are related to thermodynamics by Eq. (2.10). Analogously to the $\lambda$ line in $^3$He-$^4$He mixtures [22,23], $k_1$, $k_2$, and the ratio of the two $\gamma$ couplings are related to derivatives along the critical line, which are smooth functions of the temperature and can therefore be considered as constants in the critical region. As a consequence, both couplings must have the same critical temperature behavior in order to obtain a constant ratio. The corresponding thermodynamic expressions are listed in Table VII.

The thermodynamic expressions for the correlation functions are determined from the first-order response of the local density function to small variations of the intensive external fields [3]. They have been summarized in Table VIII.

The transformation matrix introduced in Eq. (2.29) may

TABLE VI. Thermodynamic identification of the background parameters $a_{ij}$ at the plait point and at the consolute point.

| Parameter | PP | CP |
|---|---|---|
| $a_{11}$ | $\frac{\rho}{RT}\left(\frac{\partial\Delta}{\partial c}\right)^{(0)}_{\sigma,\rho}$ | $\frac{\rho}{RT}\left(\frac{\partial T}{\partial\sigma}\right)^{(0)}_{c,\rho}$ |
| $a_{22}$ | $\frac{1}{RT\rho}\left(\frac{\partial P}{\partial\rho}\right)^{(0)}_{\sigma,c}$ | $\frac{1}{RT\rho}\left(\frac{\partial P}{\partial\rho}\right)^{(0)}_{\sigma,c}$ |
| $a_{12}$ | $\frac{\rho}{RT}\left(\frac{\partial\Delta}{\partial\rho}\right)^{(0)}_{\sigma,c}$ | $\frac{\rho}{RT}\left(\frac{\partial T}{\partial\rho}\right)^{(0)}_{\sigma,c}$ |
| | $\frac{1}{RT\rho}\left(\frac{\partial P}{\partial c}\right)^{(0)}_{\sigma,\rho}$ | $\frac{1}{RT_\rho}\left(\frac{\partial P}{\partial\sigma}\right)^{(0)}_{c,\rho}$ |

be expressed by thermodynamic derivatives along the critical line. Inserting the thermodynamic expressions from Table VII into the transformation matrix (2.30) the matrix elements are determined by finite critical line derivatives. The result has been listed in Table IX, where a concentration susceptibility at $T_c$

$$\chi_{\sigma,T_c}=\left(\frac{\partial c}{\partial\Delta}\right)_{\sigma,T_c}+\frac{1}{\rho^2}\left(\frac{\partial P}{\partial\Delta}\right)_{\sigma,T_c}\left(\frac{\partial\rho}{\partial\Delta}\right)_{\sigma,T_c} \tag{A1}$$

and a parameter $C_{c,T_c}$ representing some kind of specific heat at $T_c$

$$C_{c,T_c}=T\left[\left(\frac{\partial\sigma}{\partial T}\right)_{c,T_c}+\frac{1}{\rho^2}\left(\frac{\partial P}{\partial T}\right)_{c,T_c}\left(\frac{\partial\rho}{\partial T}\right)_{c,T_c}\right] \tag{A2}$$

have been introduced. From the background parameters in Table VI, the correlation functions in Table VIII, and the transformation matrix in Table IX thermodynamic expressions of the transformed correlation functions (2.32) and (2.33) can be calculated, which are at the plait point

$$\langle\mathring{m}_1\mathring{m}_1\rangle_c=\frac{RT}{\rho}\,\chi_{\sigma,T_c}, \tag{A3}$$

$$\langle\mathring{m}_2\mathring{m}_2\rangle_c=RT\rho^3\left(\frac{\partial\Delta}{\partial P}\right)^2_{\sigma,T_c}\left[\left(\frac{\partial c}{\partial\Delta}\right)_{\sigma,P}-\left(\frac{\partial c}{\partial\Delta}\right)^2_{\sigma,T_c}\chi^{-1}_{\sigma,T_c}\right] \tag{A4}$$

and at the consolute point

TABLE VII. Thermodynamic equivalents of the constants $k_1, k_2$ introduced in Eq. (2.10) and the ratio $\mathring{\gamma}_1/\mathring{\gamma}_2$ at the plait point and at the consolute point.

| Parameter | PP | CP |
|---|---|---|
| $k_1$ | $\frac{\rho}{RT}\left(\frac{\partial\Delta}{\partial c}\right)_{\sigma,T_c}$ | $\frac{\rho}{RT}\left(\frac{\partial T}{\partial\sigma}\right)_{c,T_c}$ |
| $k_2$ | $\frac{1}{\rho RT}\left(\frac{\partial P}{\partial\rho}\right)_{\sigma,T_c}$ | $\frac{1}{\rho RT}\left(\frac{\partial P}{\partial\rho}\right)_{c,T_c}$ |
| $\frac{\mathring{\gamma}_1}{\mathring{\gamma}_2}$ | $-\left(\frac{\partial\rho}{\partial c}\right)_{\sigma,T_c}$ | $-\left(\frac{\partial\rho}{\partial\sigma}\right)_{c,T_c}$ |

TABLE VIII. Correspondence between the correlations and the thermodynamic derivatives at the two critical points.

| Cumulant | PP | CP |
|---|---|---|
| $\langle\phi_0\phi_0\rangle_c$ | $\frac{RT}{\rho}\left(\frac{\partial\sigma}{\partial T}\right)_{\Delta,P}$ | $\frac{RT}{\rho}\left(\frac{\partial c}{\partial\Delta}\right)_{T,P}$ |
| $\langle\mathring{q}_1\mathring{q}_1\rangle_c$ | $\frac{RT}{\rho}\left(\frac{\partial c}{\partial\Delta}\right)_{\sigma,P}$ | $\frac{RT}{\rho}\left(\frac{\partial\sigma}{\partial T}\right)_{c,P}$ |
| $\langle\mathring{q}_2\mathring{q}_2\rangle_c$ | $RT\rho\left(\frac{\partial\rho}{\partial P}\right)_{\sigma,\Delta}$ | $RT\rho\left(\frac{\partial\rho}{\partial P}\right)_{c,T}$ |
| $\langle\mathring{q}_1\mathring{q}_2\rangle_c$ | $\frac{RT}{\rho}\left(\frac{\partial\rho}{\partial\Delta}\right)_{\sigma,P}$ | $\frac{RT}{\rho}\left(\frac{\partial\rho}{\partial T}\right)_{c,P}$ |
| | $RT\rho\left(\frac{\partial c}{\partial P}\right)_{\sigma,\Delta}$ | $RT\rho\left(\frac{\partial\sigma}{\partial P}\right)_{c,T}$ |

$$\langle\mathring{m}_1\mathring{m}_1\rangle_c=\frac{R}{\rho}\,C_{c,T_c}, \tag{A5}$$

$$\langle\mathring{m}_2\mathring{m}_2\rangle_c=RT\rho^3\left(\frac{\partial T}{\partial P}\right)^2_{c,T_c}\left[\left(\frac{\partial\sigma}{\partial T}\right)_{c,P}-\left(\frac{\partial\sigma}{\partial T}\right)^2_{c,T_c}TC^{-1}_{c,T_c}\right]. \tag{A6}$$

## APPENDIX B: DYNAMIC FUNCTIONAL AND VERTEX FUNCTIONS

The calculation of dynamic correlation functions or dynamic vertex functions correspondingly in a perturbation series requires a generating dynamic functional. The basic way to obtain such a functional from a set of dynamic equations, which include stochastic forces, has been shown in [27] for the dynamics of ferromagnets. In this treatment the essential presumptions were that first all equations contain fluctuating forces and second these forces are stochastically independent, which means that the corresponding matrix of Onsager coefficients is not singular. However, the hydrodynamic equations include the continuity equation for the mass density, which is an exact relation expressing the conservation of mass and therefore do not contain any fluctuating force. Nevertheless, it is possible to extend the treatment to a mixed set of dynamic equations consisting of stochastic and exact

TABLE IX. Thermodynamic expressions of the transformation matrix (2.29).

| Coefficient | PP | CP |
|---|---|---|
| $M_{11}$ | 1 | 1 |
| $M_{22}$ | $\chi^{-1}_{\sigma,T_c}\left(\frac{\partial c}{\partial\Delta}\right)_{\sigma,T_c}$ | $TC^{-1}_{c,T_c}\left(\frac{\partial\sigma}{\partial T}\right)_{c,T_c}$ |
| $M_{12}$ | $\frac{1}{\rho^2}\left(\frac{\partial P}{\partial\Delta}\right)_{\sigma,T_c}$ | $\frac{1}{\rho^2}\left(\frac{\partial P}{\partial T}\right)_{c,T_c}$ |
| $M_{21}$ | $-\chi^{-1}_{\sigma,T_c}\left(\frac{\partial\rho}{\partial\Delta}\right)_{\sigma,T_c}$ | $-TC^{-1}_{c,T_c}\left(\frac{\partial\rho}{\partial T}\right)_{c,T_c}$ |

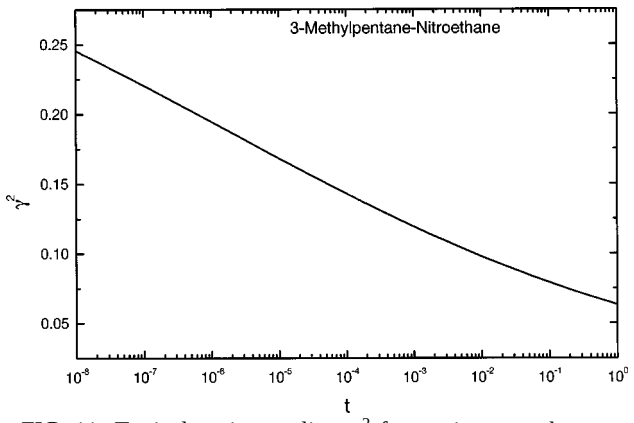


FIG. 11. Typical static coupling $\gamma^2$ for a mixture at the consolute point.

equations. For the hydrodynamic equations of pure fluids this has been shown in explicitly [1]. Let us assume that we have $N$ densities $\alpha_i$, $i=1,...,N$, with the dynamic equation

$$\partial_t \vec{\alpha} = \vec{V} + \vec{\Theta} \tag{B1}$$

containing stochastically independent fluctuating forces $\Theta_i$ (in liquid mixtures this would be $\sigma$, $c$, $\boldsymbol{j}_l$, and $\boldsymbol{j}_l$) and $M$ densities $a_i$, $i=1,\ldots,N$, fulfilling the exact relation

$$\partial_t \vec{a} = \vec{W} \tag{B2}$$

(in liquid mixtures this would be $\rho$). The fluctuating forces fulfill the Einstein relation

$$\langle \vec{\Theta}(x,t) \otimes \vec{\Theta}(x',t') \rangle = -2 \overleftrightarrow{\Lambda}' \nabla^2 \delta(x-x') \delta(t-t'), \tag{B3}$$

where $\overleftrightarrow{\Lambda}'$ is a $N \times N$ nonsingular matrix. The coefficients of this matrix result from the corresponding hydrodynamic equations. $\vec{V}$ and $\vec{W}$ generally are functions of the densities $\alpha_i$ and $a_i$. The exact relations (B2) may be considered as secondary conditions on the generating functional, which means that the stochastic forces fluctuate in such a way that Eq. (B2) is always fulfilled. Thus the generating functional can be written as

$$Z_d = \int \prod_{i=1}^{N} \mathcal{D}(\Theta_i) \prod_{j=1}^{M} \mathcal{D}(F_j)\, \delta(F_j) \times \exp\left[ -\frac{1}{4} \int dt\, dx\, \vec{\Theta}^T \overleftrightarrow{\Lambda}'^{-1} \vec{\Theta} \right], \tag{B4}$$

with $F_j = \partial_t a_j - W_j$. $\mathcal{D}$ refers to a suitable integration measure. Inserting Eq. (B1) and changing the integration variables from $\Theta_i$ to $\alpha_i$ leads to

$$Z_d = \int \prod_{i=1}^{N} \mathcal{D}(\alpha_i) \prod_{j=1}^{M} \mathcal{D}(a_j)\, \delta(\partial_t a_j - W_j) \times \exp\left[ -\frac{1}{4} \int dt \int dx \left( [\partial_t \vec{\alpha} - \vec{V}]^T \times \overleftrightarrow{\Lambda}'^{-1} [\partial_t \vec{\alpha} - \vec{V}] + 2 \sum_i^N \frac{\delta V_i}{\delta \alpha_i} + 2 \sum_j^M \frac{\delta W_j}{\delta a_j} \right) \right]. \tag{B5}$$

The $\delta$ function may be expressed by an exponential function

$$\delta(\partial_t a_j - W_j) = \int \mathcal{D}(i\tilde{a}_j) \exp\left[ -\int dx \int dt\ \tilde{a}_j (\partial_t a_j - W_j) \right]. \tag{B6}$$

Performing a Gaussian transformation where also auxiliary fields $\tilde{\alpha}_i$ are introduced, Eq. (B5) turns into

$$Z_d = \int \int \prod_{i=1}^{N} \mathcal{D}(\alpha_i, i\tilde{\alpha}_i) \prod_{j=1}^{M} \mathcal{D}(a_j, i\tilde{a}_j) e^{-J}, \tag{B7}$$

with

$$J = \int dt \int dx \left( -\vec{\tilde{\alpha}}^T \overleftrightarrow{\Lambda}' \vec{\tilde{\alpha}} + \vec{\tilde{\alpha}}^T (\partial_t \vec{\alpha} - \vec{V}) + \vec{\tilde{a}}^T (\partial_t \vec{a} - \vec{W}) + \frac{1}{2} \sum_i^N \frac{\delta V_i}{\delta \alpha_i} + \frac{1}{2} \sum_{j=1}^M \frac{\delta W_j}{\delta a_j} \right). \tag{B8}$$

Especially in liquid mixtures, the above dynamic functional corresponds to dynamic equations for $\sigma$, $c$, $\rho$, $\boldsymbol{j}_l'$, and $\boldsymbol{j}_t'$. Introducing the order parameter (2.1) or (2.2), respectively, and the secondary densities (2.3), we obtain the dynamic equations (2.12)–(2.15) containing fluctuating forces. However, these are not independent, which is expressed by the relations (2.20) between the Onsager coefficients leading to the singular matrix $[\Lambda_{ij}]$ (singular in the sense that no inverse matrix exists) defined in Eq. (2.17). The order parameter and the secondary densities may also be introduced in the dynamic functional (B8). This leads to the dynamic functional

$$J = \int dt \int dx \left( -[\tilde{\beta}_i]^T [\Lambda_{ij}] [\tilde{\beta}_j] + [\tilde{\beta}_i]^T (\partial_t [\beta_j] - [\mathcal{V}_j]) + \frac{1}{2} \sum_i \frac{\delta \mathcal{V}_i}{\delta \beta_i} \right), \tag{B9}$$

where $[\beta_i]$ is defined by $[\beta_i]^T = (\phi_0, \mathring{q}_1, \mathring{q}_2, \boldsymbol{j}_l, \boldsymbol{j}_t)$ ($[\tilde{\beta}_i]$ is defined analogously with the corresponding auxiliary densities) and $[\Lambda_{ij}]$ is the coefficient matrix (2.17). Further, we have introduced $[\mathcal{V}_i]^T = (\vec{V}^T, \vec{W}^T)$. The structure of the functional (B9) is same as for the case where only dynamic equations with stochastic independent fluctuating forces are considered. The fact that now exact relations are included is considered in the properties of $[\Lambda_{ij}]$, which is now a singular (not invertable) matrix. An explicit expression for Eq. (B9) is obtained inserting the dynamic equations (2.12)–(2.15). The Fourier transformed Gaussian part can be written as

$$J^{(0)}=\frac{1}{2}\int_{k,\omega}\{[\beta_i]^T(k,\omega),[\tilde{\beta}_i]^T(k,\omega)\}\times\mathring{\mathbf{\Gamma}}^{(0)}(k,\omega)\begin{pmatrix}[\beta_j](-k,-\omega)\\ [\tilde{\beta}_j](-k,-\omega)\end{pmatrix}. \tag{B10}$$

The integration is defined as $\int_{k,\omega}=\int[d^dk/(2\pi)^d]\int(d\omega/2\pi)$. The elements of the matrix $\mathring{\mathbf{\Gamma}}^{(0)}(k,\omega)$ are the dynamic vertex functions in lowest-order perturbation theory. They are given explicitly by

$$\mathring{\mathbf{\Gamma}}^{(0)}(k,\omega)=\begin{pmatrix}[0] & -i\omega[1]+[\mathring{L}_{\alpha\tilde{\beta}}](k)\\ i\omega[1]+[\mathring{L}_{\tilde{\alpha}\beta}](k) & -2[\lambda_{\tilde{\alpha}\tilde{\beta}}](k)\end{pmatrix}, \tag{B11}$$

where $[1]$ denotes the unit matrix. Further, we have $[\mathring{L}_{\tilde{\alpha}\beta}](k)=[\mathring{L}_{\alpha\tilde{\beta}}]^\dagger(k)$, where the dagger superscript denotes the adjoint matrix. The submatrices are given by

$$[\mathring{L}_{\alpha\tilde{\beta}}](k)=\begin{pmatrix}\mathring{\Gamma}k^2(\mathring{\tau}+k^2) & \mathring{L}k^2(\mathring{\tau}+k^2) & \mathring{L}_\phi k^2(\mathring{\tau}+k^2) & -ik\mathring{g}_l\mathring{h}_2 & 0\\ (a_{11}\mathring{L}+a_{12}\mathring{L}_\phi)k^2 & (a_{11}\mathring{\mu}+a_{12}\mathring{L}_{12})k^2 & (a_{11}\mathring{L}_{12}+a_{12}\mathring{\lambda})k^2 & ika_{12}\mathring{c} & 0\\ (a_{12}\mathring{L}+a_{22}\mathring{L}_\phi)k^2 & (a_{12}\mathring{\mu}+a_{22}\mathring{L}_{12})k^2 & (a_{12}\mathring{L}_{12}+a_{22}\mathring{\lambda})k^2 & ika_{22}\mathring{c} & 0\\ 0 & 0 & ika_j\mathring{c} & a_j\mathring{\lambda}_lk^2 & 0\\ 0 & 0 & 0 & 0 & a_j\mathring{\lambda}_tk^2\end{pmatrix}, \tag{B12}$$

$$[\lambda_{\tilde{\alpha}\tilde{\beta}}](k)=\begin{pmatrix}\mathring{\Gamma}k^2 & \mathring{L}k^2 & \mathring{L}_\phi k^2 & 0 & 0\\ \mathring{L}k^2 & \mathring{\mu}k^2 & \mathring{L}_{12}k^2 & 0 & 0\\ \mathring{L}_\phi k^2 & \mathring{L}_{12}k^2 & \mathring{\lambda}k^2 & 0 & 0\\ 0 & 0 & 0 & \mathring{\lambda}_lk^2 & 0\\ 0 & 0 & 0 & 0 & \mathring{\lambda}_tk^2\end{pmatrix}. \tag{B13}$$

The interaction terms in the Hamiltonian (2.4) and the mode coupling terms in the dynamic equation modify the matrix (B11) and may be calculated in a perturbation expansion. Generally, the matrix of the dynamic two-point vertex function is given by

$$\mathbf{\Gamma}(k,\omega)=\mathbf{\Gamma}^{(0)}(k,\omega)-\mathbf{\Sigma}(k,\omega), \tag{B14}$$

where $\Sigma(k,\omega)$ contains 1-irreducible diagrams with two external legs. The matrix $\mathring{\mathbf{\Gamma}}(k,\omega)$ of the vertex functions has the structure

$$\mathring{\mathbf{\Gamma}}(k,\omega)=\begin{pmatrix}[0] & [\mathring{\Gamma}_{\alpha,\tilde{\beta}}](k,\omega)\\ [\mathring{\Gamma}_{\tilde{\alpha},\beta}](k,\omega) & [\mathring{\Gamma}_{\tilde{\alpha},\tilde{\beta}}](k,\omega)\end{pmatrix}, \tag{B15}$$

with the submatrix

$$[\mathring{\Gamma}_{\alpha\tilde{\beta}}]=\begin{pmatrix}\mathring{\Gamma}_{\phi\tilde{\phi}} & \mathring{\Gamma}_{\phi\tilde{q}_1} & \mathring{\Gamma}_{\phi\tilde{q}_2} & \mathring{\Gamma}_{\phi\tilde{l}} & 0\\ \mathring{\Gamma}_{q_1\tilde{\phi}} & \mathring{\Gamma}_{q_1\tilde{q}_1} & \mathring{\Gamma}_{q_1\tilde{q}_2} & \mathring{\Gamma}_{q_1\tilde{l}} & 0\\ \mathring{\Gamma}_{q_2\tilde{\phi}} & \mathring{\Gamma}_{q_2\tilde{q}_1} & \mathring{\Gamma}_{q_2\tilde{q}_2} & \mathring{\Gamma}_{q_2\tilde{l}} & 0\\ \mathring{\Gamma}_{l\tilde{\phi}} & \mathring{\Gamma}_{l\tilde{q}_1} & \mathring{\Gamma}_{l\tilde{q}_2} & \mathring{\Gamma}_{q\tilde{l}} & 0\\ 0 & 0 & 0 & 0 & \mathring{\Gamma}_{tt}\end{pmatrix}. \tag{B16}$$

The submatrices $[\mathring{\Gamma}_{\tilde{\alpha},\beta}]$ and $[\mathring{\Gamma}_{\tilde{\alpha},\tilde{\beta}}]$ are defined analogously. The propagators of the model are determined inverting Eq. (B11). Within the model the hydrodynamic structure is contained in the dynamic two-point vertex functions, which are calculated in perturbation expansion. Some details and definitions are summarized in Appendix B. Because the considered structures are invariant under the transformation (2.29), the following expressions are generally formulated independently of which secondary densities ($\vec{q}_0$ or $\vec{m}_0$) are used. This is indicated by indices $\alpha_i$, for which one may insert $q_i$

or $m_i$. The dynamic two-point vertex functions have the structure

$$[\mathring{\Gamma}_{\alpha\tilde{\beta}}]=\begin{pmatrix} -i\omega[\underline{1}]+k^2[\mathring{\underline{F}}_{\alpha\tilde{\alpha}}] & k[\mathring{G}_{\alpha}] & [0] \\ k[\mathring{G}_{\tilde{\alpha}}]^T & -i\omega+k^2\mathring{f}_{l\tilde{l}} & 0 \\ [0]^T & 0 & -i\omega+k^2\mathring{f}_{t\tilde{t}} \end{pmatrix}, \tag{B17}$$

with three-dimensional submatrices and vectors defined as

$$[\mathring{\underline{F}}_{\alpha\tilde{\alpha}}]=\begin{pmatrix} \mathring{f}_{\phi\tilde{\phi}} & \mathring{\vec{F}}^T_{\tilde{\alpha}} \\ \mathring{\vec{F}}_{\alpha} & \mathring{\vec{\vec{F}}}_{\alpha\tilde{\alpha}} \end{pmatrix}, \quad [\mathring{G}_{\alpha}]=\begin{pmatrix} \mathring{g}_{\phi\tilde{l}} \\ \mathring{g}_{\alpha_1\tilde{l}} \\ \mathring{g}_{\alpha_2\tilde{l}} \end{pmatrix},$$

$$[\mathring{G}_{\tilde{\alpha}}]=\begin{pmatrix} \mathring{g}_{l\tilde{\phi}} \\ \mathring{g}_{l\tilde{\alpha}_1} \\ \mathring{g}_{l\tilde{\alpha}_2} \end{pmatrix}. \tag{B18}$$

The matrices and vectors contained in $[\mathring{\underline{F}}_{\alpha\tilde{\alpha}}]$ are defined in the two-dimensional secondary density space by

$$\mathring{\vec{\vec{F}}}_{\alpha\tilde{\alpha}}=\begin{pmatrix} \mathring{f}_{\alpha_1\tilde{\alpha}_1} & \mathring{f}_{\alpha_1\tilde{\alpha}_2} \\ \mathring{f}_{\alpha_2\tilde{\alpha}_1} & \mathring{f}_{\alpha_2\tilde{\alpha}_2} \end{pmatrix}, \quad \mathring{\vec{F}}_{\alpha}=\begin{pmatrix} \mathring{f}_{\alpha_1\tilde{\phi}} \\ \mathring{f}_{\alpha_2\tilde{\phi}} \end{pmatrix}, \quad \mathring{\vec{F}}_{\tilde{\alpha}}=\begin{pmatrix} \mathring{f}_{\phi\tilde{\alpha}_1} \\ \mathring{f}_{\phi\tilde{\alpha}_2} \end{pmatrix}. \tag{B19}$$

$[\underline{1}]$ in Eq. (B17) is the three-dimensional unit matrix and $[0]$ is a three-dimensional null vector. The functions $\mathring{f}_{\alpha_i\tilde{\alpha}_j}$ and $\mathring{g}_{\alpha_i\tilde{l}}$ or $\mathring{g}_{l\tilde{\alpha}_i}$ denote the $k^2$ and $k$ contributions to the vertex functions at wave vector $k=0$,

$$\mathring{f}_{\alpha_i\tilde{\alpha}_j}=\frac{\partial}{\partial k^2}\,\mathring{\Gamma}_{\alpha_i\tilde{\alpha}_j}|_{k=0}, \quad \mathring{g}_{\alpha_i\tilde{l}}=\frac{\partial}{\partial k}\,\mathring{\Gamma}_{\alpha_i\tilde{l}}|_{k=0},$$

$$\mathring{g}_{l\tilde{\alpha}_i}=\frac{\partial}{\partial k}\,\mathring{\Gamma}_{l\tilde{\alpha}_i}|_{k=0}. \tag{B20}$$

Generally, these functions depend on the frequency, the temperature, the Onsager coefficients, and the static and dynamic couplings. They may be calculated in perturbation expansion by summing one-particle irreducible graphical contributions with two corresponding external legs. Analogously to pure fluids [1], the functions in Eq. (B18) separate into purely dynamic functions $[\mathring{\underline{F}}^{(d)}_{\alpha\tilde{\alpha}}]$, $[\mathring{G}^{(d)}_{\alpha}]$, and $[\mathring{G}^{(d)}_{\tilde{\alpha}}]$, in which all contributions due to perturbation expansion are proportional to the mode coupling parameters and frequency-dependent functions $[\mathring{\underline{\Gamma}}_{\alpha\alpha}]$ that reduce to the static two-point vertex functions $[\mathring{\underline{\Gamma}}^{(s)}_{\alpha\alpha}]=[\mathring{\underline{\Gamma}}_{\alpha\alpha}]$ $(\omega=0)$ in the limit of zero frequency. Thus Eq. (B18) can be written as

$$[\mathring{\underline{F}}_{\alpha\tilde{\alpha}}]=[\mathring{\underline{\Gamma}}_{\alpha\alpha}][\mathring{\underline{F}}^{(d)}_{\alpha\tilde{\alpha}}], \quad [\mathring{G}_{\alpha}]=[\mathring{\underline{\Gamma}}_{\alpha\alpha}][\mathring{G}^{(d)}_{\alpha}],$$

$$[\mathring{G}_{\tilde{\alpha}}]=a_j[\mathring{G}^{(d)}_{\tilde{\alpha}}] \tag{B21}$$

where $[\mathring{\underline{F}}^{(d)}_{\alpha\tilde{\alpha}}]$ has the same structure as in Eq. (B18) with a superscript $(d)$ at all functions and

$$[\mathring{\underline{\Gamma}}_{\alpha\alpha}]=\begin{pmatrix} \mathring{\Gamma}_{\phi\phi} & \vec{0}^T \\ \vec{0} & \mathring{\vec{\vec{\Gamma}}}_{\alpha\alpha} \end{pmatrix}, \quad \mathring{\vec{\vec{\Gamma}}}_{\alpha\alpha}=\begin{pmatrix} \mathring{\Gamma}_{\alpha_1\alpha_1} & \mathring{\Gamma}_{\alpha_1\alpha_2} \\ \mathring{\Gamma}_{\alpha_1\alpha_2} & \mathring{\Gamma}_{\alpha_2\alpha_2} \end{pmatrix}. \tag{B22}$$

The secondary densities $\vec{m}_0$ are decoupled; therefore, in these variables the cross vertex function $\mathring{\Gamma}_{m_1m_2}=0$ and the matrix (B22) is of diagonal structure.

## APPENDIX C: EXPLICIT EXPRESSIONS FOR $\mathring{c}\to\infty$

Due to the invariance of the determinant (3.10) under transformation (2.29), the explicit appearance of dynamic vertex functions in Eqs. (3.11)–(3.30) is the same in variables $\vec{q}_0$ as well as in $\vec{m}_0$. In the limit $\mathring{c}\to\infty$ this changes because of the different behavior of the vectors $[\mathring{G}_{\alpha}]$ and $[\mathring{G}_{\tilde{\alpha}}]$. The functions $\mathring{g}_{\phi\tilde{l}}$ and $\mathring{g}_{l\tilde{\phi}}$ do not contain a factor $\mathring{c}$ and therefore can be neglected. Independently of the secondary densities, both functions $\mathring{g}_{\alpha_2\tilde{l}}$ and $\mathring{g}_{l\tilde{\alpha}_2}$ are proportional to $\mathring{c}$. Differences in the two sets of secondary densities arise in the vertex functions $\mathring{g}_{\alpha_1\tilde{l}}$ and $\mathring{g}_{l\tilde{\alpha}_1}$. For the secondary densities $\vec{q}_0$ the vertex functions behave like $\mathring{g}_{q_1\tilde{l}}\sim O(\mathring{c})$ and $\mathring{g}_{l\tilde{q}_1}\sim O(1)$. Thus the vectors in Eq. (B18) can be written as

$$\lim_{\mathring{c}\to\infty}[\mathring{G}_q]=\begin{pmatrix} 0 \\ \mathring{g}_{q_1\tilde{l}} \\ \mathring{g}_{q_2\tilde{l}} \end{pmatrix}, \quad \lim_{\mathring{c}\to\infty}[\mathring{G}_{\tilde{q}}]=\begin{pmatrix} 0 \\ 0 \\ \mathring{g}_{l\tilde{q}_2} \end{pmatrix}. \tag{C1}$$

For the secondary densities $\vec{m}_0$ one has $\mathring{g}_{m_1\tilde{l}}\sim O(\mathring{c})$ and $\mathring{g}_{l\tilde{m}_1}\sim O(\mathring{c})$. Thus the vectors $[\mathring{G}_{\tilde{\alpha}}]$ and $[\mathring{G}_{\alpha}]$ in Eq. (B18) reduce to

$$\lim_{\mathring{c}\to\infty}[\mathring{G}_m]=\begin{pmatrix} 0 \\ \mathring{g}_{m_1\tilde{l}} \\ \mathring{g}_{m_2\tilde{l}} \end{pmatrix}, \quad \lim_{\mathring{c}\to\infty}[\mathring{G}_{\tilde{m}}]=\begin{pmatrix} 0 \\ \mathring{g}_{l\tilde{m}_1} \\ \mathring{g}_{l\tilde{m}_2} \end{pmatrix}, \tag{C2}$$

when only $\mathring{c}\to\infty$ contributions are considered. The expressions (3.11), (3.12), (3.16), and (3.28) reduce to

$$\lim_{\mathring{c}\to\infty} \mathcal{C}_s^2 = -\mathring{g}_{q_2\tilde{l}}\mathring{g}_{l\tilde{q}_2} = -(\mathring{g}_{m_1\tilde{l}}\mathring{g}_{l\tilde{m}_1} + \mathring{g}_{m_2\tilde{l}}\mathring{g}_{l\tilde{m}_2}), \tag{C3}$$

$$\lim_{\mathring{c}\to\infty} \mathcal{D}_s = \mathring{f}_{l\tilde{l}} + \mathring{f}_{q_2\tilde{q}_2} + \mathring{f}_{q_2\tilde{q}_1}\frac{\mathring{g}_{q_1\tilde{l}}}{\mathring{g}_{q_2\tilde{l}}} = \mathring{f}_{l\tilde{l}} + \frac{\mathring{g}_{m_1\tilde{l}}\mathring{g}_{l\tilde{m}_1}\mathring{f}_{m_1\tilde{m}_1} + \mathring{g}_{m_2\tilde{l}}\mathring{g}_{l\tilde{m}_2}\mathring{f}_{m_2\tilde{m}_2} + \mathring{g}_{m_1\tilde{l}}\mathring{g}_{l\tilde{m}_2}\mathring{f}_{m_2\tilde{m}_1} + \mathring{g}_{m_2\tilde{l}}\mathring{g}_{l\tilde{m}_1}\mathring{f}_{m_1\tilde{m}_2}}{\mathring{g}_{m_1\tilde{l}}\mathring{g}_{l\tilde{m}_1} + \mathring{g}_{m_2\tilde{l}}\mathring{g}_{l\tilde{m}_2}}, \tag{C4}$$

$$\lim_{\mathring{c}\to\infty} \mathring{\mathcal{F}}_{\alpha\tilde{\alpha}} = \mathring{f}_{q_1\tilde{q}_1} - \mathring{f}_{q_2\tilde{q}_1}\frac{\mathring{g}_{q_1\tilde{l}}}{\mathring{g}_{q_2\tilde{l}}} = \frac{\mathring{g}_{m_1\tilde{l}}\mathring{g}_{l\tilde{m}_1}\mathring{f}_{m_2\tilde{m}_2} + \mathring{g}_{m_2\tilde{l}}\mathring{g}_{l\tilde{m}_2}\mathring{f}_{m_1\tilde{m}_1} - \mathring{g}_{m_1\tilde{l}}\mathring{g}_{l\tilde{m}_2}\mathring{f}_{m_2\tilde{m}_1} - \mathring{g}_{m_2\tilde{l}}\mathring{g}_{l\tilde{m}_1}\mathring{f}_{m_1\tilde{m}_2}}{\mathring{g}_{m_1\tilde{l}}\mathring{g}_{l\tilde{m}_1} + \mathring{g}_{m_2\tilde{l}}\mathring{g}_{l\tilde{m}_2}}, \tag{C5}$$

$$\lim_{\mathring{c}\to\infty} \mathcal{W}_{\alpha\tilde{\alpha}} = \mathring{f}_{\phi\tilde{q}_1}\left(\mathring{f}_{q_1\tilde{\phi}} - \mathring{f}_{q_2\tilde{\phi}}\frac{\mathring{g}_{q_1\tilde{l}}}{\mathring{g}_{q_2\tilde{l}}}\right) = \frac{\mathring{g}_{m_1\tilde{l}}\mathring{g}_{l\tilde{m}_1}\mathring{f}_{\phi\tilde{m}_2}\mathring{f}_{m_2\tilde{\phi}} + \mathring{g}_{m_2\tilde{l}}\mathring{g}_{l\tilde{m}_2}\mathring{f}_{\phi\tilde{m}_1}\mathring{f}_{m_1\tilde{\phi}} - \mathring{g}_{m_1\tilde{l}}\mathring{g}_{l\tilde{m}_2}\mathring{f}_{\phi\tilde{m}_1}\mathring{f}_{m_2\tilde{\phi}} - \mathring{g}_{m_2\tilde{l}}\mathring{g}_{l\tilde{m}_1}\mathring{f}_{\phi\tilde{m}_2}\mathring{f}_{m_1\tilde{\phi}}}{\mathring{g}_{m_1\tilde{l}}\mathring{g}_{l\tilde{m}_1} + \mathring{g}_{m_2\tilde{l}}\mathring{g}_{l\tilde{m}_2}}. \tag{C6}$$

All functions in Eqs. (C3) and (3.28) are calculated in perturbation expansion, which simplifies in the limit $\mathring{c}\to\infty$. From the structure of the perturbational contributions two general statements, valid in all orders of the perturbation expansion, can be made.

(i) No contributions to the purely dynamic parts $[\mathring{G}_{\tilde{\alpha}}^{(d)}]$ and $[\mathring{G}_{\alpha}^{(d)}]$ introduced in Eq. (B21) arise from the perturbation expansion. Thus one simply has

$$[\mathring{G}_q^{(d)}] = [\mathring{G}_{\tilde{q}}^{(d)}] = \begin{pmatrix} 0 \\ 0 \\ i\mathring{c} \end{pmatrix}, \quad [\mathring{G}_m^{(d)}] = [\mathring{G}_{\tilde{m}}^{(d)}] = \begin{pmatrix} 0 \\ i\mathring{c}_1 \\ i\mathring{c}_2 \end{pmatrix}. \tag{C7}$$

The perturbation expansion contributes only to the vertex functions $[\mathring{\underline{\Gamma}}_{\alpha\alpha}]$, which may be considered as frequency-dependent extensions of the static vertex functions. The resulting matrices are

$$[\mathring{\underline{\Gamma}}_{qq}] = \begin{pmatrix} \mathring{\Gamma}_{\phi\phi}(\omega) & 0 & 0 \\ 0 & \mathring{\Gamma}_{q_1q_1}(\omega) & \mathring{\Gamma}_{q_1q_2}(\omega) \\ 0 & \mathring{\Gamma}_{q_1q_2}(\omega) & \mathring{\Gamma}_{q_2q_2}(\omega) \end{pmatrix}, \tag{C8}$$

$$[\mathring{\underline{\Gamma}}_{mm}] = \begin{pmatrix} \mathring{\Gamma}_{\phi\phi}(\omega) & 0 & 0 \\ 0 & a_1 & 0 \\ 0 & 0 & \mathring{\Gamma}_{m_2m_2}(\omega) \end{pmatrix}. \tag{C9}$$

(ii) Also in the matrix $[\mathring{\underline{F}}_{\alpha\tilde{\alpha}}^{(d)}]$ all functions do not get any contributions from the mode couplings, except the order parameter function $\mathring{f}_{\phi\tilde{\phi}}^{(d)}$. Therefore, one may write

$$[\mathring{\underline{F}}_{q\tilde{q}}^{(d)}] = \begin{pmatrix} \mathring{f}_{\phi\tilde{\phi}}^{(d)}(\omega) & \mathring{L} & \mathring{L}_{\phi} \\ \mathring{L} & \mathring{\mu} & \mathring{L}_{12} \\ \mathring{L} & \mathring{L}_{12} & \mathring{\lambda} \end{pmatrix},$$

$$[\mathring{\underline{F}}_{m\tilde{m}}^{(d)}] = \begin{pmatrix} \mathring{f}_{\phi\tilde{\phi}}^{(d)}(\omega) & \mathring{L} & \mathring{L}_{\phi} \\ \mathring{L} & \mathring{\mu} & \mathring{L}_{12} \\ \mathring{L}_{\phi} & \mathring{L}_{12} & \mathring{\lambda} \end{pmatrix}. \tag{C10}$$

## APPENDIX D: RENORMALIZATION OF THE STATIC AND DYNAMIC PARAMETERS

One advantage of the introduction of the transformed densities $\vec{m}_0$ in Eq. (2.29) is that the whole renormalization procedure concerning the parameters appearing also in mixtures is equal to the procedure in pure fluids, which have been considered extensively in [1]. Therefore, we give here only a short summary of the basic definitions and relations. The renormalization will be performed within the field theoretic renormalization group theory. With the minimal subtraction scheme [56] dimensional singularities at space dimension $d=4$ in the vertex functions will be absorbed into $Z$ factors.

Within statics the momentum density and the density $\mathring{m}_1$ appearing in Eq. (2.31) do not need renormalization. The remaining densities $\phi_0$ and $\mathring{m}_2$ in Eq. (2.31) and the corresponding model parameters renormalize analogously to $\phi_0$ and $q_0$ in pure fluids [1]. The order parameter and the second secondary field are renormalized by

$$\phi_0 = Z_{\phi}^{1/2}\phi, \quad \mathring{m}_2 = Z_{m_2}^{1/2}m_2, \tag{D1}$$

where $Z_{m_2}$ is determined by the singularities of the $\phi^2$-$\phi^2$ correlation function and can be written as

$$Z_{m_2}^{-1} = 1 + \gamma^2 A(u). \tag{D2}$$

$A(u)$ contains the singularities of the specific heat calculated within the $\phi^4$ model and is obtained by an additive renormalization of the $\phi^2$-$\phi^2$ correlation function. $u$ is the renormalized fourth-order coupling of the $\phi^4$ model (2.6) in which renormalized parameters will be introduced by

$$\mathring{r} - \mathring{r}_c = Z_{\phi}^{-1}Z_r r, \quad \mathring{u} = \kappa^{\epsilon}Z_{\phi}^{-2}Z_u u A_d^{-1}. \tag{D3}$$

$\kappa$ is the reference wave number and $\epsilon=d-4$. The factor $A_d=\Gamma(3-d/2)/2^{d-2}\pi^{d/2}(d-2)$ has been chosen for convenience to obtain a minimal number of perturbation contributions in an $\epsilon$ expansion of the specific heat [24]. The $\epsilon$ singularities connected with the remaining parameter $\mathring{\gamma}_m$ in Eq. (2.31) can also be absorbed in renormalization factors defined in the $\phi^4$ model by

$$\mathring{\gamma}_m=\kappa^{\epsilon/2}Z_\phi^{-1}Z_{m_2}^{1/2}Z_r\gamma_m A_d^{-1/2}. \tag{D4}$$

From the $Z$ factors we introduce the $\zeta$ functions

$$\zeta_i=\left(\kappa\frac{\partial\ln Z_i^{-1}}{\partial\kappa}\right)_0,\quad i=\phi,q,r,u. \tag{D5}$$

The index 0 in Eq. (D5) indicates that the derivative is taken at fixed unrenormalized parameters. The fixed point values $\zeta_i^*$ of the $\zeta$ functions at the Heisenberg fixed point are related to the critical exponents by

$$\zeta_\phi^*=-\eta,\quad \zeta_{m_2}^*=\frac{\alpha}{\nu},\quad \zeta_r^*-\zeta_\phi^*=2-\frac{1}{\nu}. \tag{D6}$$

The static vertex functions can be expressed by renormalized parameters with

$$\mathring{\Gamma}^{(s)}_{\phi\phi}(\xi^{-2},\mathring{u})=(\kappa l)^2Z_\phi^{-1}\exp\left(\int_1^l\frac{dx}{x}\,\zeta_\phi\right)\hat{\Gamma}^{(s)}_{\phi\phi}(u(l)), \tag{D7}$$

$$\mathring{\Gamma}^{(s)}_{m_2m_2}(\xi^{-2},\mathring{\gamma}^2,\mathring{u})=Z_{m_2}^{-1}\exp\left(\int_1^l\frac{dx}{x}\,\zeta_{m_2}\right)\hat{\Gamma}^{(s)}_{m_2m_2}(\gamma^2(l),u(l)). \tag{D8}$$

The coupling $\gamma^2$ has been defined in Eq. (3.47). The amplitude function $\hat{\Gamma}^{(s)}_{\phi\phi}$ corresponds to the inverse order parameter correlation of the $\phi^4$ model. The secondary density amplitude function can be written as

$$\hat{\Gamma}^{(s)}_{m_2m_2}(\gamma^2(l),u(l))=\frac{a_2}{1+\gamma^2(l)F_+^{(s)}(u(l))}, \tag{D9}$$

where $F_+^{(s)}(u(l))$ is the amplitude of the $\langle\phi^2\phi^2\rangle_c$ correlation function also calculated within the $\phi^4$ model [24].

In dynamics all hydrodynamic densities are conserved. Therefore, the conjugated densities $\tilde{\phi}_0$ and $\mathring{\tilde{m}}_2$ introduced in the dynamic functional (B7) do not require an independent dynamic renormalization. Thus we have

$$\tilde{\phi}_0=Z_\phi^{-1/2}\tilde{\phi},\quad \mathring{\tilde{m}}_2=Z_{m_2}^{-1/2}\tilde{m}_2. \tag{D10}$$

As a consequence of the Galilean invariance of the equations of motion, the mode couplings do not need independent $Z$ factors. The following renormalized couplings will be introduced:

$$\mathring{g}=\kappa^{1+\epsilon/2}gA_d^{-1/2},\quad \mathring{\vec{g}}_l=\kappa^{2+\epsilon/2}\vec{g}_lA_d^{-1/2}. \tag{D11}$$

The Onsager coefficients renormalize as

$$\mathring{\Gamma}=Z_\phi Z_\Gamma^{(d)}\Gamma,\quad \mathring{\hat{L}}_\phi=\kappa Z_\phi^{1/2}Z_{m_2}^{1/2}\hat{L}_\phi,\quad \mathring{\hat{\lambda}}=\kappa^2Z_{m_2}\hat{\lambda}, \tag{D12}$$

$$\mathring{\lambda}_l=\kappa^2Z_{\lambda_l}\lambda_l,\quad \mathring{\lambda}_t=\kappa^2Z_{\lambda_t}\lambda_t. \tag{D13}$$

In mixtures the additional Onsager coefficients

$$\mathring{\hat{\mu}}=\kappa^2\hat{\mu},\quad \mathring{\hat{L}}=\kappa^2Z_\phi^{1/2}\hat{L},\quad \mathring{\hat{L}}_{12}=\kappa^2Z_{m_2}^{1/2}\hat{L}_{12} \tag{D14}$$

appear. From the above relations one can see that only $\Gamma$, $\lambda_l$, and $\lambda_t$ have independent dynamic $Z$ factors, while the renormalization of the remaining coefficients is completely determined by statics. $Z_\Gamma^{(d)}$, $Z_{\lambda_l}$, and $Z_{\lambda_t}$ in Eqs. (D12) and (D13) do not contain static $\epsilon$ poles. The couplings $\mathring{c}_1$ and $\mathring{c}_2$ renormalize as

$$\mathring{c}_1=\kappa^3c_1,\quad \mathring{c}_2=\kappa^3Z_{m_2}^{1/2}c_2. \tag{D15}$$

We define $\zeta$ functions for $i=\Gamma,\hat{L}_\phi,\hat{\lambda},\hat{L},\hat{\mu},\hat{L}_{12},\lambda_l,\lambda_t$ analogously to Eq. (D5). The critical temperature dependence of the Onsager coefficients is determined by the flow equations

$$l\frac{d\Gamma}{dl}=\Gamma(\zeta_\Gamma^{(d)}+\zeta_\phi),\quad l\frac{d\hat{\lambda}}{dl}=\hat{\lambda}(-2+\zeta_{m_2}), \tag{D16}$$

$$l\frac{d\hat{L}_\phi}{dl}=\hat{L}_\phi\left(-1+\frac{1}{2}\,\zeta_\phi+\frac{1}{2}\,\zeta_{m_2}\right), \tag{D17}$$

$$l\frac{d\lambda_l}{dl}=\lambda_l(-2+\zeta_{\lambda_l}),\quad l\frac{d\lambda_t}{dl}=\lambda_t(-2+\zeta_{\lambda_t}). \tag{D18}$$

The additional Onsager coefficients in mixtures behave as

$$l\frac{d\hat{\mu}}{dl}=-2\hat{\mu},\quad l\frac{d\hat{L}}{dl}=\left(-1+\frac{1}{2}\,\zeta_\phi\right)\hat{L},$$

$$l\frac{d\hat{L}_{12}}{dl}=\left(-2+\frac{1}{2}\,\zeta_{m_2}\right)\hat{L}_{12}. \tag{D19}$$

The corresponding flow equation for the couplings $c_1$ and $c_2$ are

$$l\frac{dc_1}{dl}=-3c_1,\quad l\frac{dc_2}{dl}=c_2\left(-3+\frac{1}{2}\,\zeta_{m_2}\right). \tag{D20}$$

From Eqs. (D16) and (D19) the flow equation

TABLE X. One-loop expressions of the dynamic $\zeta$ functions and amplitude functions for liquids and mixtures.

| Function | Liquid | Mixture |
|---|---|---|
| $\zeta_\Gamma^{(d)}$ | $-3/4f_t^2$ | $-3/4f_t^2$ |
| $\zeta_{\lambda_t}$ | $-\frac{f_t^2}{24}$ | $-\frac{f_t^2}{24(1-w_3^2)}$ |
| $G$ | $-\frac{f_t^2}{16}$ | $-\frac{f_t^2}{16}$ |
| $E_t$ | $-\frac{f_t^2}{36}$ | $-\frac{f_t^2}{36(1-w_3^2)}$ |

$$l\,\frac{dw_3}{dl}=-\frac{1}{2}\,w_3\zeta_\Gamma^{(d)} \tag{D21}$$

follows for the time scale ratio introduced in Eq. (3.37), which implies immediately the fixed point value $w_3^*=0$. The mode coupling parameter $f_t$ defined in Eq. (4.5) fulfills the equation

$$l\,\frac{df_t}{dl}=-\frac{1}{2}\,f_t(\epsilon+\zeta_\Gamma^{(d)}+\zeta_{\lambda_t}+\zeta_\phi). \tag{D22}$$

Because of $w_3^*=0$, $\zeta_\Gamma^{(d)*}$ and $\zeta_{\lambda_t}^*$ are same values as in pure fluids. As a consequence, also the fixed point value of the mode coupling parameter $f_t^*$ is identical to the one in pure fluids.

## APPENDIX E: ONE-LOOP EXPRESSIONS

In this appendix we will briefly summarize the explicit results for all functions that are calculated in a perturbation expansion in one-loop order. The static $\zeta$ functions and amplitude functions are the same as for pure fluids [1] because the additional density $m_1$ enters only quadratic in (2.31) and therefore does not contribute to the perturbation expansion. The one-loop expressions are

$$\zeta_\phi=0,\quad \zeta_r=\frac{u}{2},\quad \zeta_{m_2}=\frac{\gamma^2}{2},\quad \zeta_u=\frac{3}{2}\,u, \tag{E1}$$

$$F_+^{(s)}(u)=-\frac{1}{4},\quad \hat{\Gamma}_{\phi\phi}^{(s)}(u)=1,\quad B_{\phi^2}=\frac{1}{2}. \tag{E2}$$

The one-loop results for the dynamic $\zeta$ functions and the dynamic zero-frequency amplitude functions are listed in Table X. In order to allow a comparison we have given these functions for pure liquids and for mixtures.

At finite frequencies the one-loop expression of $F_+(v,\tilde{w})$ is given by

$$F_+(v,\tilde{w})=-\frac{1}{4}\left\{\frac{v^2}{v_+v_-}\ln v+\frac{1}{v_+-v_-}\left[\frac{v_-^2}{v_+}\ln v_--\frac{v_+^2}{v_-}\ln v_+\right]\right\}, \tag{E3}$$

where we have introduced

$$v_\pm=\frac{v}{2}\pm\sqrt{\left(\frac{v}{2}\right)^2+i\tilde{w}}. \tag{E4}$$

The amplitude functions $E_t(v,\tilde{w})$ and $E_l(v,\tilde{w})$ are the same as given in [1] [see Eqs. (5.5) and (5.24) therein] for pure fluids, when one replaces $w$ and $f_t^2$ there by $\tilde{w}$ and $f_t^2/(1-w_3^2)$. For this reason we do not repeat the lengthy one-loop expressions in this context.


[1] R. Folk and G. Moser, Phys. Rev. E **57**, 683 (1998); **57**, 705 (1998).
[2] E. D. Siggia, B. I. Halperin, and P. C. Hohenberg, Phys. Rev. B **13**, 2110 (1976).
[3] R. Folk and G. Moser, J. Low Temp. Phys. **99**, 11 (1995).
[4] V. Privman, P. C. Hohenberg, and A. Aharony, in *Phase Transitions and Critical Phenomena*, edited by C. Domb and J. L. Lebowitz (Academic, London, 1991), Vol. 14.
[5] J. Luettmer-Strathmann and J. V. Sengers, J. Chem. Phys. **104**, 3026 (1996).
[6] S. B. Kiselev and M. L. Huber, Fluid Phase Equilibria **142**, 253 (1998).
[7] S. B. Kiselev and V. D. Kulikov, Int. J. Thermophys. **18**, 1143 (1997).
[8] S. B. Kiselev and V. D. Kulikov, Int. J. Thermophys. **15**, 283 (1993).
[9] M. A. Anisimov and S. B. Kiselev, Int. J. Thermophys. **13**, 873 (1992).
[10] R. Folk and G. Moser, Europhys. Lett. **24**, 533 (1993).
[11] R. Folk and G. Moser, Int. J. Thermophys. **16**, 1363 (1995).
[12] R. Folk and G. Moser, Phys. Rev. Lett. **75**, 2706 (1995).
[13] R. Folk and G. Moser, Int. J. Thermophys. (to be published).
[14] R. A. Ferrell and J. K. Bhattacharjee, Phys. Rev. B **24**, 4095 (1981).
[15] R. A. Ferrell and J. K. Bhattacharjee, Phys. Rev. A **31**, 1788 (1985).
[16] D. M. Kroll and J. M. Ruhland, Phys. Rev. A **23**, 371 (1981).
[17] K. Kawasaki, Phys. Rev. A **1**, 1750 (1970).
[18] A. Onuki, J. Phys. Soc. Jpn. **66**, 511 (1997).
[19] R. Folk and G. Moser, Europhys. Lett. **41**, 177 (1998).
[20] J. Pankert and V. Dohm, Phys. Rev. B **40**, 10 842 (1989); **40**, 10 856 (1989).
[21] D. N. Zubarev, *Nonequilibrium Statistical Thermodynamics* (Plenum, New York, 1974).
[22] A. Onuki, J. Low Temp. Phys. **53**, 1 (1983).
[23] G. Moser and R. Folk, J. Low Temp. Phys. **86**, 57 (1992); **86**, 99 (1992).
[24] V. Dohm, Z. Phys. B **60**, 61 (1985).
[25] I. E. Dzyaloshinskii and G. E. Volovick, Ann. Phys. (N.Y.) **125**, 67 (1980).
[26] L. D. Landau and E. M. Lifshitz, *Fluid Mechanics*, 2nd ed. (Pergamon, New York, 1987).
[27] R. Bausch, H. K. Janssen, and H. Wagner, Z. Phys. B **24**, 113 (1976).
[28] M. A. Anisimov, E. E. Gorodetskii, V. D. Kulikov, A. A. Povodyrev, and J. V. Sengers, Physica A **220**, 277 (1995).
[29] R. B. Griffith and J. C. Wheeler, Phys. Rev. A **2**, 1047 (1970).
[30] T. Doiron, D. Gestrich, and H. Meyer, Phys. Rev. B **22**, 3202 (1980).
[31] G. Moser and V. Dohm (unpublished).
[32] H. Meyer and L. H. Cohen, Phys. Rev. A **38**, 2081 (1988).
[33] B. Wallace, Jr. and H. Meyer, Phys. Rev. A **5**, 953 (1972).
[34] G. R. Brown and H. Meyer, Phys. Rev. A **6**, 1578 (1972).
[35] T. Doiron, R. P. Behringer, and H. Meyer, J. Low Temp. Phys. **24**, 345 (1976).
[36] L. H. Cohen, M. L. Dingus, and H. Meyer, Phys. Rev. Lett. **50**, 1058 (1983).

[37] L. H. Cohen, M. L. Dingus, and H. Meyer, J. Low Temp. Phys. **61**, 79 (1985).
[38] Y. Miura, H. Meyer, and A. Ikushima, J. Low Temp. Phys. **55**, 247 (1984).
[39] R. Folk and G. Moser, Condens. Matter Phys **7**, 27 (1996).
[40] M. Giglio and A. Vendramini, Phys. Rev. Lett. **34**, 561 (1975).
[41] R. A. Ferrell, Int. J. Thermophys. **10**, 369 (1989).
[42] R. A. Ferrell, Phys. Rev. Lett. **24**, 1169 (1970); R. Perl and R. A. Ferrell, Phys. Rev. A **6**, 2358 (1972).
[43] W. Mayer, S. Hoffmann, G. Meier, and I. Alig, Phys. Rev. E **55**, 3102 (1997).
[44] E. Bittmann, I. Alig, and D. Woermann, Ber. Bunsenges. Phys. Chem. **98**, 189 (1994).
[45] J. K. Bhattacharjee and R. A. Ferrell, Physica A **250**, 83 (1998).
[46] D. Beysens, *Proceedings of the 1980 Cargése Summer Institute on Phase Transitions*, edited by M. Lévy, J.-C. Le Guillou, and J. Zinn-Justin (Plenum, New York, 1982).
[47] G. Paladin and L. Peliti, J. Phys. (France) Lett. **43**, 15 (1982); **45**, 289(E) (1984).
[48] Hong Hao, Ph.D. thesis, University of Maryland, 1991 (unpublished) [cited in J. Luettmer-Strathmann, J. V. Sengers, and G. A. Olchowy, J. Chem. Phys. **103**, 7482 (1995)].
[49] R. F. Berg and M. R. Moldover, J. Chem. Phys. **93**, 1926 (1990); Phys. Rev. A **42**, 7183 (1990).
[50] G. Flossmann, R. Folk, and G. Moser (unpublished).
[51] E. Sakonidou, H. R. van den Berg, C. A. ten Seldam, and J. V. Sengers, Phys. Rev. E **56**, R4943 (1997); J. Chem. Phys. **109**, 717 (1998).
[52] W. Mayer, S. Hoffmann, G. Meier, and I. Alig, Phys. Rev. E **55**, 3102 (1997).
[53] Y. B. Melnichenko, M. A. Anisimov, A. A. Povodyrev, G. D. Wignall, J. V. Sengers, and W. A. Van Hook, Phys. Rev. Lett. **79**, 5266 (1997).
[54] G. Meier, B. Momper, and E. W. Fischer, J. Chem. Phys. **97**, 5884 (1992).
[55] R. F. Berg and K. Gruner, J. Chem. Phys. **101**, 1513 (1994).
[56] D. J. Amit, *Field Theory, The Renormalization Group and Critical Phenomena*, 2nd ed. (World Scientific, Singapore, 1984).
[57] D. Atack and O. K. Rice, J. Chem. Phys. **22**, 382 (1954).
[58] S. Wang and H. Meyer, J. Low Temp. Phys. **69**, 377 (1987).
[59] G. Arcovito, C. Faloci, M. Roberti, and L. Mistura, Phys. Rev. Lett. **22**, 1040 (1969).